

BREAKDOWN OF ROTATIONAL TORI IN 2D AND 4D CONSERVATIVE AND DISSIPATIVE STANDARD MAPS

ADRIAN P. BUSTAMANTE, ALESSANDRA CELLETTI, AND CHRISTOPH LHOTKA

ABSTRACT. We study the breakdown of rotational invariant tori in 2D and 4D standard maps by implementing three different methods. First, we analyze the domains of analyticity of a torus with given frequency through the computation of the Lindstedt series expansions of the embedding of the torus and the drift term. The Padé and log-Padé approximants provide the shape of the analyticity domains by plotting the poles of the polynomial at the denominator of the Padé approximants. Secondly, we implement a Newton method to construct the embedding of the torus; the breakdown threshold is then estimated by looking at the blow-up of the Sobolev norms of the embedding. Finally, we implement an extension of Greene method to get information on the breakdown threshold of an invariant torus with irrational frequency by looking at the stability of the periodic orbits with periods approximating the frequency of the torus.

We apply these methods to 2D and 4D standard maps. The 2D maps can either be conservative (symplectic) or dissipative (more precisely, conformally symplectic, namely a dissipative map with the geometric property to transform the symplectic form into a multiple of itself). The conformally symplectic maps depend on a dissipative parameter and a drift term, which is needed to get the existence of invariant attractors. The 4D maps are obtained coupling (i) two symplectic standard maps, or (ii) two conformally symplectic standard maps, or (iii) a symplectic and a conformally symplectic standard map.

Concerning the results, Padé and Newton methods perform well and provide reliable and consistent results (although we implemented Newton method only for symplectic and conformally symplectic maps). Our implementation of the extension of Greene method is inconclusive, since it is computationally expensive and delicate, especially in 4D non-symplectic maps, also due to the existence of Arnold tongues.

Keywords. Symplectic systems, Conformally symplectic systems, Dissipative systems, Standard map, Invariant tori, Periodic Orbits, Padé approximants, Greene method, Lindstedt series, Newton method, Arnold tongues.

1. INTRODUCTION

1.1. The goal of the work. As a motivation for studying 2D and 4D conservative and dissipative maps, we mention that in low-dimensional systems (e.g. Hamiltonian

Corresponding author: *E-mail address:* celletti@mat.uniroma2.it.

A.C. and C.L. acknowledge EU H2020 MSCA ETN Stardust-R Grant Agreement 813644. A.B. and C.L. acknowledge the MIUR Excellence Department Project awarded to the Department of Mathematics, University of Rome Tor Vergata, CUP E83C23000330006, and the project MIUR-PRIN 20178CJA2B “New Frontiers of Celestial Mechanics: theory and Applications”. C.L. acknowledges GNFM/INdAM.

systems with less or equal than 2 d.o.f.) invariant rotational tori provide a strong stability property, since they divide the phase space into invariant regions. In higher dimensional systems, the confinement is no more valid and the orbits can go around the invariant tori, a well-studied phenomenon known as *Arnold diffusion* ([1]). In Celestial Mechanics, an example of low-dimensional system described by a Hamiltonian with 2 d.o.f. is given by the planar, circular, restricted three-body problem. Taking a surface of section on a given energy level, one obtains a 2D map. Releasing the assumption of circular orbits and allowing the orbits of the primaries to be elliptic, one obtains that the motion takes place in a 6D phase space. Taking a surface of section on a given energy level, one obtains a 4D map.

It is worth mentioning that dissipative effects in Celestial Mechanics are found at different size scales; we just quote Poynting-Robertson drag on small particles, the effect of the atmosphere on Earth's satellites, tidal torques on planetary satellites. Such effects greatly contribute to shaping the evolution of objects in the solar system.

Given this physical motivation, the breakdown of invariant tori (namely, tori whose dynamics is smoothly conjugated to a rotation) in conservative and dissipative 2D and 4D maps is the core subject of the current work. Before proceeding, let us specify what we mean by breakdown of invariant tori. The maps we are going to study are nearly-integrable and depend on a perturbing parameter, say ε , such that the map is integrable when $\varepsilon = 0$ and it is non-integrable when $\varepsilon \neq 0$. An invariant torus with a fixed irrational frequency (precisely, Diophantine), say ω , exists in the integrable case. The torus gets deformed when ε increases, until a critical value, say ε_c , is reached at which point the invariant torus breaks down. We will implement different methods to compute ε_c . We notice that in the dissipative case, one needs to introduce a drift parameter (see [42], [10], [13]).

1.2. Maps and frequencies. We will consider conservative and dissipative maps. In particular, we start from the 2D standard map introduced by Chirikov in [25], which is an area-preserving map, and hence symplectic; we study also its dissipative version, obtained adding a dissipative parameter and a drift term. We will consider also 4D maps by coupling two 2D symplectic maps, thus obtaining the 4D symplectic map, known as the *Froeschlé map*. Next, we consider the coupling of a symplectic and a dissipative 2D map, providing what we call a *mixed* 4D map, depending on a dissipative parameter and a 1D drift term. Finally, we consider the coupling of two 2D dissipative maps, which generate a dissipative 4D map, depending on two dissipative parameters and two drift

terms. When the dissipative parameters are equal, the map is said conformally symplectic ([14]), which means that it is a dissipative map with the property that it transforms the symplectic form into a multiple of itself.

We will mainly consider the classical standard map with only one harmonic, but we will also provide a few results for maps with two harmonics.

In the 2D maps, the 1D invariant tori are labeled by a scalar irrational frequency. KAM theory ([37], [2], [41]) assumes that the irrational frequency satisfies a Diophantine condition. One can construct rational approximants to the frequency by taking the truncations of the continued fraction expansion of the irrational number. Each rational approximant corresponds to a periodic orbit, that approximates better the invariant torus as the period gets longer. In the 4D maps, the 2D invariant tori are labeled by a frequency vector with two components; in this case, the construction of the rational approximants is more elaborate, see, e.g., [36], [43], [45], [44]. We will implement the so-called Jacobi-Perron algorithm, which gives an explicit procedure to construct rational approximants to the 2D frequency vector of the 4D symplectic, mixed, dissipative standard maps.

1.3. Computing the breakdown threshold. In this work, we implement three different methods (to which we refer as Padé approximants, Newton method, Greene method) to determine the breakdown threshold of rotational invariant tori. Let us briefly detail such methods.

Invariant tori are represented by an embedding function and one needs to compute also a drift term in the dissipative case. The embedding and the drift can be expanded in Lindstedt series, in powers of the perturbing parameter. The terms of the Lindstedt series can be obtained through recursive formulae as solutions of suitable cohomological equations. We compute these terms up to a given order and then we determine the Padé approximants of the truncated series, namely polynomials whose quotients have the same Taylor expansions as the truncation (see [11], [12] for computations concerning the dissipative 2D standard map). The locations of the zeros of the polynomial at the denominator provide an approximation of the analyticity domain of the invariant tori in the complex parameter plane. Pioneer works on the computation of Lindstedt series, analyticity domains and breakdown of tori are provided by [33], where the 2D standard map is studied, and [8], [38], where the 4D semi-standard map is analyzed. The shape and size of the analyticity domain strongly depends on the nature of the map and the characteristics of the frequency. We compute also the logarithmic Padé approximants ([28]), which complement the results obtained by computing the Padé approximants.

Finally, we determine the radii of convergence of the Lindstedt series, which give a lower bound of the breakdown threshold of the invariant tori.

The Newton method allows us to construct an invariant torus for symplectic and conformally symplectic maps through a quadratically convergent procedure. In conformally symplectic systems, starting from the invariance equation for the embedding and the drift, the Newton method relies on the so-called *automatic reducibility* ([26], [14]), according to which, in the vicinity of an invariant torus, there exists an explicit change of coordinates that transforms the linearization of the invariance equation for the torus into a constant coefficient equation. We implement an explicit algorithm, borrowed from [14], to implement a Newton method to determine the embedding and the drift. Then, we compute the corresponding Sobolev norms, whose blow-up provides an estimate of the breakdown threshold of a torus with fixed frequency. In fact, as already noticed and implemented in [13], [21] (see also [16], [17]), if the torus exists, the Sobolev norms change with the perturbing parameter; but when approaching the critical threshold of the perturbing parameter, the Sobolev norms blow up. This behavior allows us to approximate the critical value of the perturbing parameter associated to the symplectic and conformally symplectic 2D and 4D maps. Rigorous results behind this method can be found in [18], [14]. We remark that for conformally symplectic systems the tori persist as normally hyperbolic invariant manifolds ([20]), so that the breakdown of the tori coincides with the breakdown of the conjugacy to rotations or the breakdown of normal hyperbolicity.

A technique to determine the critical threshold by looking at the behavior of the approximating periodic orbits was developed by J. Greene in [32], which contains an implementation for the symplectic 2D standard map (see [29], [39] for a partial justification of Greene method and [30], [31] for an application to volume-preserving maps). However, the symplectic standard map is very peculiar, since it can be written as the product of two involutions; as a consequence, the periodic orbits can be determined among the fixed points of one of these involutions. Unfortunately, this decomposition into involutions does not happen in the dissipative case, a fact that complicates enormously the determination of the periodic orbits, as already noticed in [21], requiring more computational time than Padé method or Sobolev criterion. Despite this complication, we attempt to determine periodic orbits also in the dissipative case, at the expenses of a big computational effort. Then, we implement an extension of Greene method, which is based on the study of the linearization of the periodic orbits with frequency close to the rotation number of the invariant torus. Besides the works [29], [39] providing pioneer results to justify the

symplectic case, a partial justification of an extension of Greene method for conformally symplectic and dissipative systems is given in [20], where it is proved that if a KAM torus exists, then one can get information on the spectrum of the periodic orbits with nearby frequencies; the proof requires adjusting parameters and provides information also on the width of the Arnold tongues.

1.4. Content of the work. In Section 2 we introduce the definitions of symplectic and conformally symplectic systems; in Section 3 we give explicit expressions for the 2D and 4D maps that we are going to study; in Section 4 we discuss the rational approximation to the irrational frequencies; in Section 5 we give the definition of invariant tori; we provide in Section 6 the Lindstedt series expansions of the hull functions representing the tori and we compute the Padé approximants to study the analyticity domains of the tori; Newton method to construct the invariant tori is presented in Section 7 together with an application of Sobolev criterion; some results about periodic orbits approximating the tori are described in Section 7.5.

2. SYMPLECTIC AND CONFORMALLY SYMPLECTIC SYSTEMS

We consider a discrete system f defined on a symplectic manifold $\mathcal{M} = B \times \mathbb{T}^d$, where $B \subseteq \mathbb{R}^d$ is an open, simply connected domain with smooth boundary and $d \geq 1$ denotes the number of degrees of freedom of the system. We assume that \mathcal{M} is endowed with a symplectic form Ω ; then, for any vectors $\underline{u}, \underline{v} \in \mathbb{R}^d$, one has

$$\Omega_{\underline{x}}(\underline{u}, \underline{v}) = (\underline{u}, J\underline{v}) , \tag{1}$$

where we assume that J , the matrix representing Ω at \underline{x} , is a constant matrix, as it will be the case for the models studied in this work (see Section 3). Symplectic and conformally symplectic maps have specific geometric properties as given by the following definition.

Definition 1. *A diffeomorphism $f : \mathcal{M} \rightarrow \mathcal{M}$ is conformally symplectic, if there exists a function $\lambda : \mathcal{M} \rightarrow \mathbb{R}$ such that*

$$f^*\Omega = \lambda\Omega , \tag{2}$$

where f^* denotes the pull-back of f . The diffeomorphism is symplectic if $\lambda = 1$.

It is known (see, e.g., [14]) that for $d \geq 2$, any function λ satisfying (2) must be constant. In the following, we will always consider λ constant.

The condition (2) is equivalent to

$$\Omega_{f(\underline{x})}(Df(\underline{x})\underline{u}, Df(\underline{x})\underline{v}) = \lambda\Omega_{\underline{x}}(\underline{u}, \underline{v}) , \quad \forall \underline{u}, \underline{v} \in \mathbb{R}^d .$$

Recalling (1), we have

$$(Df(\underline{x})\underline{u}, JDf(\underline{x})\underline{v}) = \lambda (\underline{u}, J\underline{v}) ,$$

which must be valid for any $\underline{u}, \underline{v}$, thus yielding

$$Df(\underline{x})^T J Df(\underline{x}) = \lambda J .$$

As remarked in [14], Definition 1 can be generalized to the case in which the phase space can be written as the product of $j \geq 2$ manifolds, say

$$\mathcal{M} = \mathcal{M}_1 \times \dots \times \mathcal{M}_j$$

with associated symplectic forms $\Omega_1, \dots, \Omega_j$, such that $\Omega = \Omega_1 \otimes \dots \otimes \Omega_j$. Then, (2) is replaced by the generalized condition

$$f^*\Omega = \lambda_1\Omega_1 \otimes \dots \otimes \lambda_j\Omega_j \tag{3}$$

with $\lambda_1, \dots, \lambda_j$ constants. Motivated by this remark, we introduce the following notion of systems with *mixed* symplectic and conformally symplectic properties; for short, we will refer to them as *mixed systems*.

Definition 2. *Let us consider a domain \mathcal{M} which can be written as $\mathcal{M} = \mathcal{M}_1 \times \dots \times \mathcal{M}_j$ with $j \geq 2$ and let $\Omega_1, \dots, \Omega_j$ be the symplectic forms on $\mathcal{M}_1, \dots, \mathcal{M}_j$. Let $f : \mathcal{M} \rightarrow \mathcal{M}$ be a diffeomorphism with conformal factors $\lambda_1, \dots, \lambda_j$ as in (3). We say that f represents a mixed system, if there exists an index $1 \leq k < j$, such that*

$$\lambda_1, \dots, \lambda_k \neq 1 , \quad \lambda_{k+1} = \dots = \lambda_j = 1 . \tag{4}$$

We will refer to *dissipative* systems, when not all $\lambda_1, \dots, \lambda_d$ are equal for $d \geq 2$, and they all are different from 1.

In the case of dissipative, conformally symplectic and mixed systems, we will consider a family of maps $f_{\underline{\mu}}$, where $\underline{\mu} \in \mathbb{R}^d$ is called the *drift parameter*. The reason for introducing extra parameters is that in the symplectic case, without the need of parameters, there exist invariant tori with different frequencies, while in the conformally symplectic case one needs to add a drift parameter vector to have the existence of invariant tori of prescribed frequency. When considering a family of maps $f_{\underline{\mu}}$, we say that $f_{\underline{\mu}}$ is conformally symplectic if it satisfies (2). Similarly, we extend to the family $f_{\underline{\mu}}$ the Definition 2 of mixed systems, whenever (4) is satisfied. Examples of symplectic, mixed, conformally symplectic maps are given in Section 3.

3. STANDARD MAPS

In this Section, we introduce 2D conservative and dissipative standard maps, and 4D symplectic, mixed, dissipative, and conformally symplectic standard maps.

3.1. Symplectic and conformally symplectic 2D standard maps. The conformally symplectic 2D standard map is defined by the discrete set of equations

$$\begin{aligned} y_{n+1} &= \lambda y_n + \mu + \varepsilon V(x_n) \\ x_{n+1} &= x_n + y_{n+1} , \end{aligned} \tag{5}$$

with $y_n \in \mathbb{R}$, $x_n \in \mathbb{T}$, $\varepsilon \geq 0$ is the perturbing parameter, $0 < \lambda \leq 1$ is the conformal factor, $\mu \in \mathbb{R}$ is the drift parameter, and V is a regular, periodic function. The determinant of the Jacobian of (5) is equal to λ . Hence, when $\lambda = 1$ and $\mu = 0$, one obtains the symplectic standard map ([25]), while for $\lambda > 0$ and $\mu \neq 0$, one obtains the conformally symplectic standard map.

3.2. Symplectic, conformally symplectic, mixed and dissipative 4D standard maps. We consider the map described by the following equations for $y_n, w_n \in \mathbb{R}$, $x_n, z_n \in \mathbb{T}$:

$$\begin{aligned} y_{n+1} &= \lambda_1 y_n + \mu_1 + \varepsilon \frac{\partial W}{\partial x}(x_n, z_n; \gamma) \\ x_{n+1} &= x_n + y_{n+1} \\ w_{n+1} &= \lambda_2 w_n + \mu_2 + \varepsilon \frac{\partial W}{\partial z}(x_n, z_n; \gamma) \\ z_{n+1} &= z_n + w_{n+1} , \end{aligned} \tag{6}$$

where $\varepsilon \geq 0$ is the perturbing parameter, $\gamma \geq 0$ is the coupling parameter, $0 < \lambda_1, \lambda_2 \leq 1$ are the conformal factors, $\mu_1, \mu_2 \in \mathbb{R}$ are the drift parameters, the function W is periodic in x_n, z_n , with zero average in both arguments. The system (6) is obtained by coupling two 2D standard maps; its Jacobian amounts to $\lambda_1 \lambda_2$. We will often consider the following expression for the function W entering in (6):

$$W(x, z; \gamma) = -\cos x - \cos z - \gamma \cos(x - z) . \tag{7}$$

We remark that the map (6) is:

- (i): symplectic, if $\lambda_1 = \lambda_2 = 1$, $\mu_1 = \mu_2 = 0$;
- (ii): conformally symplectic, if $\lambda_1 = \lambda_2 > 0$ and $\mu_1, \mu_2 \in \mathbb{R}$;
- (iii): mixed, if $\lambda_1 > 0$, $\lambda_2 = 1$, $\mu_1 \in \mathbb{R}$, $\mu_2 = 0$;
- (iv): dissipative (contractive), if $0 < \lambda_1 \neq \lambda_2 < 1$ and $\mu_1, \mu_2 \in \mathbb{R}$.

Remark 3. For practical purposes, we mention that the frequency vector $\underline{\omega} = (\omega_1, \omega_2)$ associated to an orbit of (6) can be approximated by the quantities

$$\omega_1 = \frac{1}{N_0} \sum_{j=1}^{N_0} y_j, \quad \omega_2 = \frac{1}{N_0} \sum_{j=1}^{N_0} w_j$$

for $N_0 \in \mathbb{Z}_+$ sufficiently large.

4. DIOPHANTINE VECTORS AND BEST APPROXIMATIONS

As it is well known, the existence of invariant tori can be proved by KAM theory, provided a condition on the frequency vector, say $\underline{\omega} \in \mathbb{R}^d$, is satisfied. More precisely, KAM theory requires that $\underline{\omega}$ satisfies a Diophantine condition, which is introduced as follows.

Definition 4. The frequency vector $\underline{\omega} \in \mathbb{R}^d$ is said to satisfy the Diophantine condition, if

$$|\underline{\omega} \cdot \underline{m}_1 + m_2|^{-1} \leq \nu^{-1} |\underline{m}_1|^\tau, \quad \underline{m}_1 \in \mathbb{Z}^d \setminus \{\underline{0}\}, \quad m_2 \in \mathbb{Z} \quad (8)$$

for some constants $0 < \nu \leq 1$, $\tau \geq 1$.

For $\tau > d - 1$, the set of Diophantine vectors has full Lebesgue measure in \mathbb{R}^d . For the 2D maps, the frequency is a scalar number, while for the 4D map the frequency is a 2D vector, say $\underline{\omega} = (\omega_1, \omega_2)$. By Liouville theorem ([35]), algebraic numbers satisfy the Diophantine condition with $d = 1$. We will consider the golden ratio $\varpi = \frac{\sqrt{5}-1}{2}$, which is the inverse of the solution of the quadratic equation $\varpi^2 - \varpi - 1 = 0$. We also introduce the spiral mean $s \simeq 1.32472$, which is the solution of the cubic equation $s^3 - s - 1 = 0$, and the number $\tau \simeq 1.83929$ as the solution of the cubic polynomial $\tau^3 - \tau^2 - \tau - 1 = 0$.

For the 2D maps, we mainly consider the frequencies ϖ and s^{-1} . For the 4D maps, we select the following 2D vectors:

$$\begin{aligned} \underline{\omega}_s &= (s - 1, s^{-1}) \simeq (0.3247, 0.7549), \\ \underline{\omega}_u &= (s^{-1}, s - 1) \simeq (0.7549, 0.3247), \\ \underline{\omega}_\tau &= (\tau^{-1}, \tau - 1) \simeq (0.5437, 0.8393) \\ \underline{\omega}_g &= (\varpi, s^{-1}) \simeq (0.6180, 0.7549) \\ \underline{\omega}_a &= (s^{-1}, s^{-2}) \simeq (0.7549, 0.5698) \\ \underline{\omega}_c &= \left(2(s - 1) - \frac{s^{-1}}{24}, s - 1\right) \simeq (0.6180, 0.3247). \end{aligned} \quad (9)$$

For the Diophantine property and rational approximations of 2D frequencies, we refer to the specialized literature ([36], [35], [43]). The vectors $\underline{\omega}_s, \underline{\omega}_u, \underline{\omega}_\tau$ (considered in [40], [45]) are Diophantine, being in the cubic field generated, respectively, by s and τ ; as for $\underline{\omega}_g$, we have verified numerically that it satisfies the Diophantine inequality (8) up to $|\underline{m}_1| + |\underline{m}_2| \leq 10^6$. The Diophantine property of $\underline{\omega}_a, \underline{\omega}_c$ has been studied in [24]. An algorithm due to Jacobi and Perron (see, e.g., [43]) to compute the rational approximants to 2D frequency vectors is briefly recalled in Appendix A.

5. INVARIANT TORI

In this Section, we introduce the definition and parametric representation of rotational KAM invariant tori for mapping systems.

Definition 5. *Let $f_{\underline{\mu}} : \mathcal{M} \rightarrow \mathcal{M}$ be a family of conformally symplectic diffeomorphisms defined on the manifold $\mathcal{M} = B \times \mathbb{T}^d$ with $B \subseteq \mathbb{R}^d$ an open, simply connected domain with smooth boundary. Let $\underline{\omega} \in \mathbb{R}^d$ be the frequency vector, satisfying the Diophantine condition (8). A KAM torus with frequency $\underline{\omega}$ is an invariant torus described by an embedding $\underline{K} : \mathcal{M} \rightarrow \mathbb{T}^d$ and a drift $\underline{\mu} \in \mathbb{R}^d$, such that the following invariance equation is satisfied:*

$$\underline{f}_{\underline{\mu}} \circ \underline{K}(\underline{\psi}) = \underline{K}(\underline{\psi} + \underline{\omega}) , \quad \underline{\psi} \in \mathbb{T}^d . \quad (10)$$

Notice that, if there exists \underline{K} satisfying (10), then $\underline{K}_{\underline{\sigma}}(\underline{\psi}) = \underline{K}(\underline{\psi} + \underline{\sigma})$ also satisfies (10) (see [14]). We also notice that, in the case of symplectic diffeomorphisms, Definition 5 applies without the need to introduce the drift term.

Let us make explicit the invariance equation (10) for the map (6). Using vector notation, we introduce the quantities

$$\underline{\xi} = (x, z) , \quad \underline{\eta} = (y, w) , \quad \underline{\lambda} = (\lambda_1, \lambda_2) , \quad \underline{\mu} = (\mu_1, \mu_2) , \quad \underline{V} = \left(\frac{\partial W}{\partial x}, \frac{\partial W}{\partial z} \right) .$$

Using the equations in (6), we obtain the relation

$$\underline{\xi}_{n+1} - (I_2 + \Lambda)\underline{\xi}_n + \Lambda\underline{\xi}_{n-1} = \underline{\mu} + \varepsilon\underline{V}(\underline{\xi}; \gamma) , \quad (11)$$

where I_2 is the 2×2 identity matrix and Λ is the diagonal 2×2 matrix with non-zero components λ_1, λ_2 .

A parameterization of an invariant torus with frequency $\underline{\omega} \in \mathbb{R}^2$ can be constructed by introducing the hull function $\underline{P} : \mathbb{T}^2 \rightarrow \mathbb{T}^2$, so that

$$\underline{\xi} = \underline{\psi} + \underline{P}(\underline{\psi}) \quad (12)$$

with the property that the flow in the parametric coordinate is linear:

$$\underline{\psi}_{n+1} = \underline{\psi}_n + 2\pi\underline{\omega} .$$

From (6), we obtain also that the components conjugated to $\underline{\xi}$ are given by

$$\underline{\eta} = \underline{\omega} + \underline{P}(\underline{\psi} + 2\pi\underline{\omega}) - \underline{P}(\underline{\psi}) .$$

From (11) and (12), we obtain that \underline{P} satisfies the following equation:

$$\begin{aligned} \underline{P}(\underline{\psi} + 2\pi\underline{\omega}) - (I_2 + \Lambda)\underline{P}(\underline{\psi}) + \Lambda\underline{P}(\underline{\psi} - 2\pi\underline{\omega}) + 2\pi(I_2 - \Lambda)\underline{\omega} \\ - \underline{\mu} - \varepsilon\underline{V}(\underline{\psi} + \underline{P}(\underline{\psi}); \gamma) = \underline{0} . \end{aligned} \quad (13)$$

As before, if \underline{P} satisfies (13), then $\underline{P}_\alpha(\underline{\psi}) := \underline{P}(\underline{\psi} + \underline{\alpha}) + \underline{\alpha}$ will also be solution of (13).

To settle this under-determinacy, we can use the normalization

$$\int_{\mathbb{T}^2} \underline{P}(\underline{\psi}) \, d\underline{\psi} = 0 . \quad (14)$$

We note that this is equivalent to the normalization used in [14]. The solution of equation (13) in the form of series expansions will be the core topic of Section 6 below. We refer to [15] for the formulation of (13) for the map (5).

6. LINDSTEDT SERIES AND ANALYTICITY DOMAINS FOR THE INVARIANT TORI

In this Section, we provide the formulae for the computation of the Lindstedt series expansions of the hull function \underline{P} introduced in (12) as well as of the drift term $\underline{\mu}$, so that they solve (13) in the sense of power series.

6.1. Iterative computation of the Lindstedt series. We start by expanding the function \underline{P} , as well as the drift $\underline{\mu}$, in power series of ε and by retaining the terms up to a given order $N \in \mathbb{Z}_+$, thus obtaining the truncated Lindstedt series:

$$\underline{P}^{(N)}(\underline{\psi}) = \sum_{j=1}^N \underline{P}_j(\underline{\psi})\varepsilon^j , \quad \underline{\mu}^{(N)} = \sum_{j=1}^N \underline{\mu}_j\varepsilon^j , \quad (15)$$

where $\underline{P}^{(N)}$ satisfies the normalization (14). Let us introduce the operator $E_{\underline{\mu}}(\underline{P})$ as the left hand side of (13). Then, we can say that $\underline{P}^{(N)}$ is such that

$$\|E_{\underline{\mu}^{(N)}}(\underline{P}^{(N)})\| = O(|\varepsilon|^{N+1}) .$$

The terms $\underline{P}_j, \underline{\mu}_j$ in (15) can be obtained as follows. Consider the formal expansion of the vector function \underline{V} as

$$\underline{V}(\underline{\psi} + \underline{P}(\underline{\psi}); \gamma) = \sum_{j=0}^{\infty} \underline{V}_j(\underline{\psi}; \gamma)\varepsilon^j; \quad (16)$$

we will give in Section 6.2 an iterative formula for the coefficients \underline{V}_j . Inserting (15) and (16) into (13), one obtains:

$$\begin{aligned} & \sum_{j=0}^{\infty} \underline{P}_j(\underline{\psi} + 2\pi\underline{\omega})\varepsilon^j - (I_2 + \Lambda) \sum_{j=0}^{\infty} \underline{P}_j(\underline{\psi})\varepsilon^j + \Lambda \sum_{j=0}^{\infty} \underline{P}_j(\underline{\psi} - 2\pi\underline{\omega})\varepsilon^j \\ & + 2\pi(I_2 - \Lambda)\underline{\omega} - \sum_{j=0}^{\infty} \underline{\mu}_j \varepsilon^j - \varepsilon \sum_{j=0}^{\infty} \underline{V}_j(\underline{\psi}; \gamma)\varepsilon^j = \underline{0} . \end{aligned}$$

From the previous relations, equating same powers of ε , the following equations are obtained for $j = 0$:

$$\underline{P}_0(\underline{\psi} + 2\pi\underline{\omega}) - (I_2 + \Lambda)\underline{P}_0(\underline{\psi}) + \Lambda\underline{P}_0(\underline{\psi} - 2\pi\underline{\omega}) + 2\pi(I_2 - \Lambda)\underline{\omega} - \underline{\mu}_0 = \underline{0} , \quad (17)$$

while for $j > 0$ the equations become:

$$\underline{P}_j(\underline{\psi} + 2\pi\underline{\omega}) - (I_2 + \Lambda)\underline{P}_j(\underline{\psi}) + \Lambda\underline{P}_j(\underline{\psi} - 2\pi\underline{\omega}) - \underline{\mu}_j = \underline{V}_{j-1}(\underline{\psi}; \gamma) . \quad (18)$$

Remark 6. Notice that, the coefficients \underline{V}_{j-1} at the right hand side of (18) depend only on the previously computed coefficients $\underline{V}_0, \underline{V}_1, \dots, \underline{V}_{j-2}$.

At the order $j = 0$, a solution of (17) is given by $\underline{P}_0 = \underline{0}$ and $\underline{\mu} = \underline{\mu}_0$ with components

$$\mu_{0,1} = 2\pi(1 - \lambda_1)\omega_1 , \quad \mu_{0,2} = 2\pi(1 - \lambda_2)\omega_2 .$$

For $j \geq 1$, the two components of the cohomology equations (18) are of the following form

$$\mathcal{L}_{\lambda, \omega} g(\underline{\psi}) - \mu = \eta(\underline{\psi}; \gamma) , \quad (19)$$

where the operator $\mathcal{L}_{\lambda, \omega}$ is defined as

$$\mathcal{L}_{\lambda, \omega} g(\underline{\psi}) := g(\underline{\psi} + 2\pi\underline{\omega}) - (1 + \lambda)g(\underline{\psi}) + \lambda g(\underline{\psi} - 2\pi\underline{\omega}) ;$$

the unknowns in (19) are the function $g : \mathbb{T}^2 \rightarrow \mathbb{R}$ and the scalar $\mu \in \mathbb{R}$, whereas the function $\eta : \mathbb{T}^2 \rightarrow \mathbb{R}$ and the parameters $\gamma, \lambda \in \mathbb{R}$ are given. The solution of (19) is obtained through the following lemma.

Lemma 7. Given $\lambda \in \mathbb{R}$, let $\underline{\omega} \in \mathbb{R}^2$ be a Diophantine vector and $\eta : \mathbb{T}^2 \rightarrow \mathbb{R}$ be an analytic function. Then, equation (19) has a unique solution (g, μ) satisfying the normalization

$$\int_{\mathbb{T}^2} g(\underline{\psi}) d\underline{\psi} = 0 , \quad (20)$$

given by

$$\begin{aligned} \mu &= -\hat{\eta}_0(\gamma) \\ g(\underline{\psi}) &= \sum_{\underline{k} \in \mathbb{Z}^2 \setminus \{0\}} \frac{\hat{\eta}_{\underline{k}}(\gamma)}{e^{2\pi i \omega \cdot \underline{k}} - (1 + \lambda) + \lambda e^{-2\pi i \omega \cdot \underline{k}}} e^{i \underline{k} \cdot \underline{\psi}}, \quad \underline{k} \neq \underline{0}, \end{aligned} \quad (21)$$

where $\hat{\eta}_{\underline{k}}(\gamma)$ are the Fourier coefficients of η .

Proof. Equation (19) can be solved in Fourier space. Consider the Fourier expansions

$$g(\underline{\psi}) = \sum_{\underline{k} \in \mathbb{Z}^2} \hat{g}_{\underline{k}} e^{i \underline{k} \cdot \underline{\psi}}, \quad \eta(\underline{\psi}; \gamma) = \sum_{\underline{k} \in \mathbb{Z}^2} \hat{\eta}_{\underline{k}}(\gamma) e^{i \underline{k} \cdot \underline{\psi}}; \quad (22)$$

inserting (22) into (19), the equation (19) becomes

$$\sum_{\underline{k} \in \mathbb{Z}^2} (e^{2\pi i \omega \cdot \underline{k}} - (1 + \lambda) + \lambda e^{-2\pi i \omega \cdot \underline{k}}) \hat{g}_{\underline{k}} e^{i \underline{\psi} \cdot \underline{k}} - \mu = \sum_{\underline{k} \in \mathbb{Z}^2} \hat{\eta}_{\underline{k}}(\gamma) e^{i \underline{\psi} \cdot \underline{k}}.$$

Its solution is given by (21). Note that \hat{g}_0 is a free parameter; we choose it in such a way that g satisfies the normalization (20), namely $\hat{g}_0 = 0$. \square

6.2. Expansions of the vector function \underline{V} . To carry out the procedure described in Section 6.1 to determine the Lindstedt series, one needs to compute the formal expansion in (16) for the function $\underline{V}(\underline{\psi} + \underline{P}(\underline{\psi}); \gamma)$, which can be found as follows (see [23]).

We consider the Fourier expansions

$$\underline{V}(\underline{\psi}; \gamma) = \sum_{\underline{k} \in \mathbb{Z}^2} \hat{V}_{\underline{k}}(\gamma) e^{i \underline{k} \cdot \underline{\psi}};$$

therefore, we obtain

$$\underline{V}(\underline{\psi} + \underline{P}(\underline{\psi}); \gamma) = \sum_{\underline{k} \in \mathbb{Z}^2} \hat{V}_{\underline{k}}(\gamma) e^{i \underline{k} \cdot (\underline{\psi} + \underline{P}(\underline{\psi}))}. \quad (23)$$

It is enough to find the expansions of the exponential functions as (compare with [9])

$$e^{i \underline{k} \cdot (\underline{\psi} + \underline{P}(\underline{\psi}))} = \sum_{j=0}^{\infty} b_{j, \underline{k}}(\underline{\psi}) \varepsilon^j \quad (24)$$

for suitable coefficients $b_{j, \underline{k}}$ which are determined as follows. Taking the derivative of both sides of (24), we obtain

$$i \underline{k} \cdot \left(\frac{d}{d\varepsilon} \underline{P}(\underline{\psi}) \right) e^{i \underline{k} \cdot (\underline{\psi} + \underline{P}(\underline{\psi}))} = \sum_{j=0}^{\infty} (j+1) b_{j+1, \underline{k}}(\underline{\psi}) \varepsilon^j.$$

Using the formal expansion of \underline{P} , together with (24), we have

$$i \underline{k} \cdot \left(\sum_{j=0}^{\infty} (j+1) \underline{P}_{j+1} \varepsilon^j \right) \sum_{j=0}^{\infty} b_{j, \underline{k}} \varepsilon^j = \sum_{j=0}^{\infty} (j+1) b_{j+1, \underline{k}} \varepsilon^j,$$

namely

$$\sum_{j=0}^{\infty} i\underline{k} \cdot \left(\sum_{h=0}^j (h+1) \underline{P}_{h+1} b_{j-h, \underline{k}} \right) \varepsilon^j = \sum_{j=0}^{\infty} (j+1) b_{j+1, \underline{k}} \varepsilon^j .$$

Thus, the following relations follow:

$$\begin{aligned} b_{0, \underline{k}}(\underline{\psi}) &= e^{i\underline{k} \cdot \underline{\psi}} \\ b_{j+1, \underline{k}}(\underline{\psi}) &= \frac{i}{j+1} \underline{k} \cdot \sum_{h=0}^j (h+1) \underline{P}_{h+1}(\underline{\psi}) b_{j-h, \underline{k}}(\underline{\psi}) , \quad j \geq 0 . \end{aligned}$$

6.3. Explicit cohomology equations. Putting together (23) and (24) one obtains that the coefficient of order ε^j in (16) is given by

$$\underline{V}_j(\underline{\varphi}; \gamma) = \sum_{\underline{k} \in \mathbb{Z}^2} \hat{V}_{\underline{k}}(\gamma) b_{j, \underline{k}}(\underline{\psi}) .$$

Thus, the explicit cohomology equations (18) at order ε^j are given by

$$\underline{P}_j(\underline{\psi} + 2\pi\underline{\omega}) - (I_2 + \Lambda) \underline{P}_j(\underline{\psi}) + \Lambda \underline{P}_j(\underline{\psi} - 2\pi\underline{\omega}) - \underline{\mu}_j = \sum_{\underline{k} \in \mathbb{Z}^2} \hat{V}_{\underline{k}}(\gamma) b_{j-1, \underline{k}}(\underline{\psi}) \quad (25)$$

whose solutions are obtained using Lemma 7. Once \underline{P}_j and $\underline{\mu}_j$ are computed from (25), one obtains the desired formal solutions $\underline{P}, \underline{\mu}$ of (13).

6.4. Analyticity domains and breakdown of attractors. In this Section, we provide some results for the 2D and 4D standard maps introduced in Section 3. Precisely, for a fixed frequency vector, say $\underline{\omega}$, we proceed along the following steps:

- A) we compute the Lindstedt series expansion up to a given order N according to the procedure described in Section 6;
- B) we analyze the behavior of the coefficients of the Lindstedt series to provide an estimate of the radius of convergence;
- C) we determine the Padé approximants (see Appendix B) associated to the Lindstedt series to order N and we draw the poles in the complex plane $(\varepsilon_r, \varepsilon_i)$.

Concerning step B), we notice that the radius of convergence ρ of the Lindstedt series in the complex ε -plane can be obtained as an approximation of

$$\rho_u(\omega) = \inf_{\theta \in \mathbb{T}} (\limsup_{n \rightarrow \infty} |u_n(\psi)|^{\frac{1}{n}})^{-1} , \quad \rho_v(\omega) = \inf_{\theta \in \mathbb{T}} (\limsup_{n \rightarrow \infty} |v_n(\psi)|^{\frac{1}{n}})^{-1} ,$$

where $\underline{P}_n = (u_n, v_n)$ are the coefficients of the formal expansion of \underline{P} in (12). For the 2D standard map in (5) it is enough to consider a hull function u satisfying

$$x = \psi + u(\psi). \quad (26)$$

In practical computations, we will compute an approximation ρ_u, ρ_v to the radius of convergence only for a specific value of the parametric coordinate, say $\bar{\psi} = 1$ in the 2D case and $\bar{\psi} = (1, 1)$ in the 4D case. In the applications for steps B) and C), the estimate of the radius of convergence is obtained by computing the limits for n large of the sequences $u_n(\bar{\psi})^{-1/n}, v_n(\bar{\psi})^{-1/n}$, while the estimate of the breakdown threshold is obtained by fitting the data to a circle and by computing the intersection of the domain with the positive real axis. When the domain presents oscillations, we indicate an inner and an outer circle. The precision of the estimate of the threshold depends on the order of the Padé approximants and we will prefer to give the results as an interval with a lower and upper limit of the threshold. We remark that the results can in principle be sharpened by increasing the order N of the Lindstedt series expansions.

6.5. Radius of convergence and Padé approximants for the 2D case. In the following case studies, the Lindstedt series in step A) are determined at different orders, up to $N = 512$, and using up to 60 digits of precision.

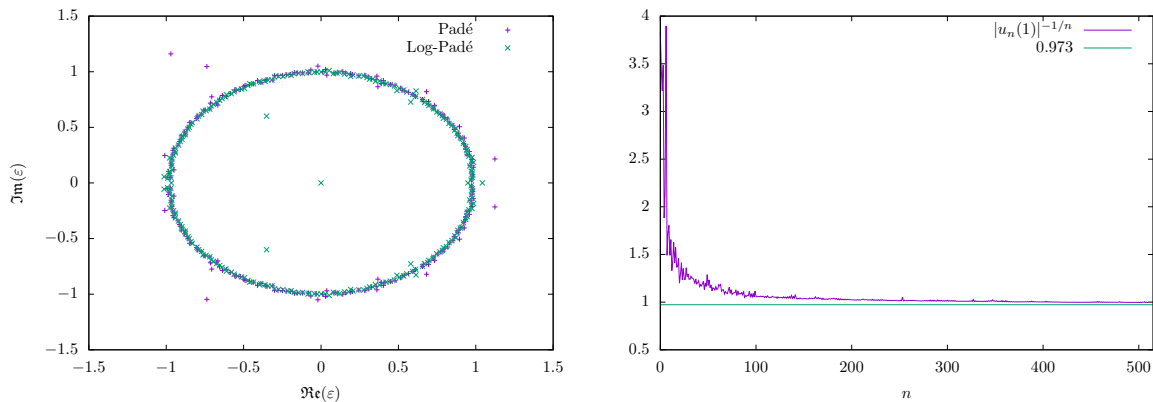


FIGURE 1. Map (5) with $V(x) = \sin x$, $\omega = \frac{\sqrt{5}-1}{2}$, $\lambda = 0.8$. Left panel: poles of Padé and log-Padé approximants with $N = 512$. Right panel: convergence of the Lindstedt series coefficients.

Figure 1 refers to the map (5) with $\omega = \frac{\sqrt{5}-1}{2}$, $\lambda = 0.8$, $V(x) = \sin x$; the left panel shows the zeros of the denominators of the Padé approximants after computing the Lindstedt series up to the order $N = 512$ and the right panel shows the values $|u_n(\bar{\psi})|^{-\frac{1}{n}}$ with $\bar{\psi} = 1$ and $n = 1, \dots, 512$. The breakdown threshold found in [13] for this sample case was $\varepsilon = 0.973$, which is consistent with the radius of convergence in the right panel of Figure 1 and with the threshold determined in the left panel of Figure 1 as the intersection of the analyticity domain with the positive abscissa (compare with [6], [28]).

It is known that the Padé approximants are better suited to approximate functions with poles, rather than functions with branch points ([5]). The theoretical and numerical evidence presented in [27], [28] indicates that the boundaries of the domains of analyticity of invariant circles could be described as an accumulation of branch points. As a consequence, a logarithmic Padé approximation (see Figure 1, left panel) is better suited to compute singularities that are branch points; we follow [28] for the computation of the logarithmic Padé approximation. More precisely, if a function $f(z)$ has a branch point singularity at $z = 1/\alpha$, then

$$f(z) = C(1 - \alpha z)^c + g(z) ,$$

where $g(z)$ is of higher order at $z = 1/\alpha$, C is a constant and $c < 0$. For z close to $1/\alpha$, one has

$$F(z) := \frac{d}{dz} \ln(f(z)) = \frac{f'(z)}{f(z)} \approx \frac{\chi}{z - (1/\alpha)} ,$$

for some $\chi \in \mathbb{R}$. The order χ of the branch point could be estimated by using Padé approximants on different functions related to $F(z)$. For example, close to $z = 1/\alpha$, one has

$$\left(z - \frac{1}{\alpha} \right) \frac{f'(z)}{f(z)} \approx \chi .$$

One expects that a Padé approximant for $F(z)$ exhibits a pole at $z = 1/\alpha$ with residue χ . Finally, to get an $[M, N]$ Padé approximant of $F(z)$ one needs to find polynomials $Q_1^{(M)}(z)$ and $Q_2^{(N)}(z)$ of degrees M and N , respectively, satisfying

$$\frac{f'(z)}{f(z)} = \frac{Q_1^{(M)}(z)}{Q_2^{(N)}(z)} + O(z^{M+N+1})$$

and $Q_2^{(N)}(0) = 1$.

Figure 2, upper plots, refers again to the 2D map in (5), but with the frequency $\omega = s^{-1}$; the left panel shows the zeros of the denominators of the Padé and log-Padé approximants for the one-harmonic case $V(x) = \sin x$ and for two values of λ ; the circles shown in Figure 2 are used to approximate the breakdown threshold and they are estimated as $\varepsilon_c \approx 0.73$ for $\lambda = 0.9$ and $\varepsilon_c \approx 0.758$ for $\lambda = 0.8$, well below the threshold of the golden ratio of Figure 1. Besides, for $\omega = s^{-1}$ the results for the domain take a sort of flower shape. The results for the two-harmonic case with $V_{2h}(x) = \sin x + \frac{1}{3} \sin(3x)$ are shown in the lower panels of Figure 2 for $\lambda = 0.8$ with $\omega = \frac{\sqrt{5}-1}{2}$ (left) and $\omega = s^{-1}$ (right). In the latter case the estimate of the threshold is more difficult, due to the irregular shape of the domain of analyticity.

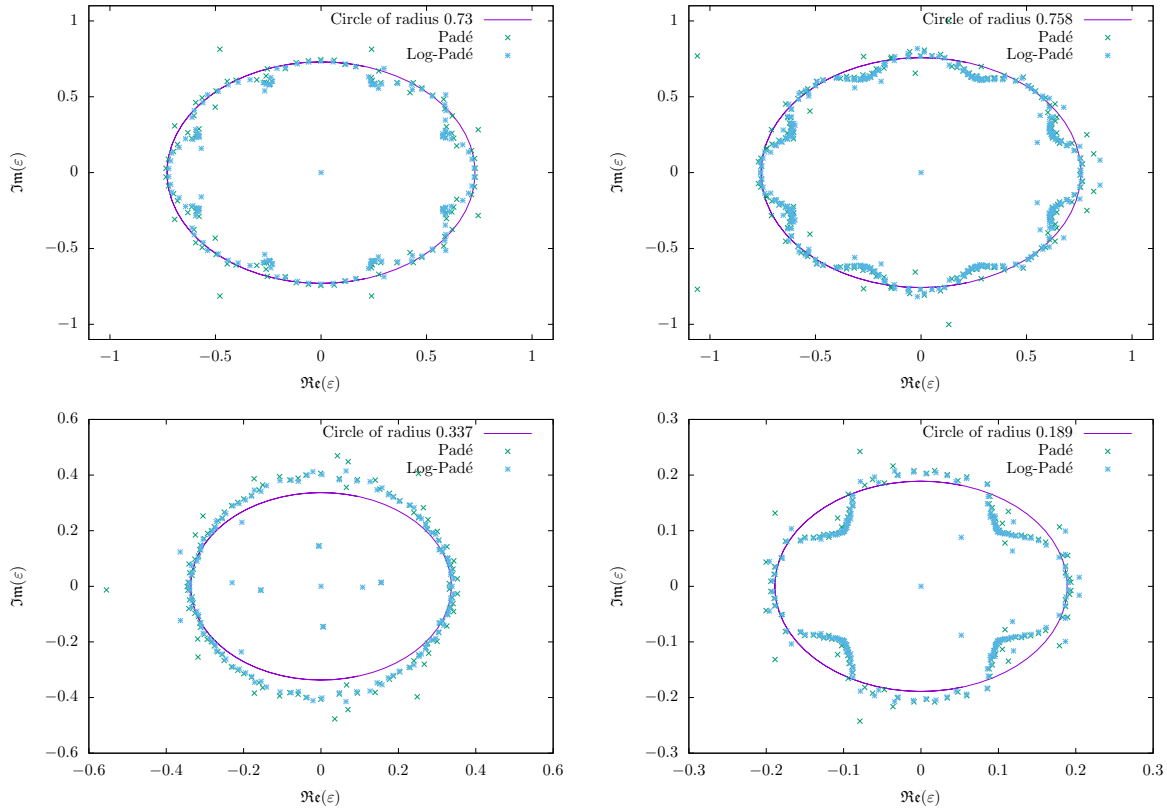


FIGURE 2. Poles of Padé and log-Padé approximants using Lindstedt series of order at least $N = 256$. Upper plots: map (5) with $V(x) = \sin(x)$, $\omega = s^{-1}$. Left: $\lambda = 0.9$, and circle of radius 0.73. Right: $\lambda = 0.8$ and circle of radius 0.758. Lower plots: map (5) with $V_{2h}(x) = \sin x + \frac{1}{3} \sin(3x)$, $\lambda = 0.8$. Left: $\omega = \frac{\sqrt{5}-1}{2}$ and circle of radius 0.337. Right: $\omega = s^{-1}$ and circle of radius 0.189.

To analyze the dependence of the domains of analyticity on the choice of the dissipation parameter λ , Figure 3 shows the results of the poles of the Padé approximants for the two harmonics potential V_{2h} and for different values of λ , taking $\omega = \frac{\sqrt{5}-1}{2}$ (left panel) and $\omega = s^{-1}$ (right panel). We fixed $N = 256$ and used 40 digits of precision; notice that the lines of poles in Figure 3 are known to be an indication of branch singularities (see [27], [28] for further details).

6.6. Padé approximants for the 4D case. For the 4D maps introduced in (6) with the potential in (7), the computations are definitely more demanding; for this reason, the Lindstedt series in step A) are determined only up to order $N = 128$, and we reach in some cases $N = 256$. Figure 4 refers to the case with $\underline{\omega}_s$, $\gamma = 0.01$; they show the poles of the Padé and log-Padé approximants with $N = 128$, obtained using 100 digits of precision,

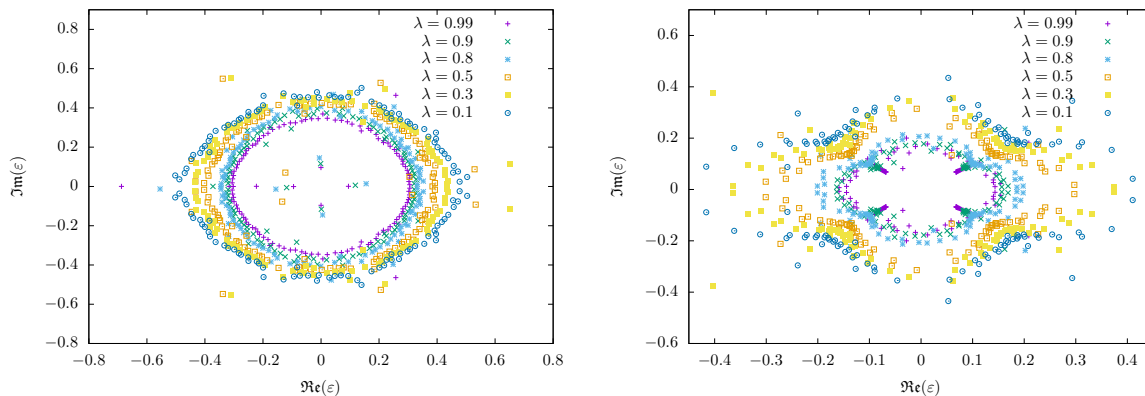


FIGURE 3. Map (5) with $V_{2h}(x) = \sin x + \frac{1}{3} \sin(3x)$ for different values of λ with $N = 256$ and 40 digits of precision. The plots display the poles of the Padé approximants for $N = 256$. Left panel: $\omega = \frac{\sqrt{5}-1}{2}$. Right panel: $\omega = s^{-1}$.

	$\underline{\omega}_s$	$\underline{\omega}_u$	$\underline{\omega}_\tau$	$\underline{\omega}_g$	$\underline{\omega}_a$	$\underline{\omega}_c$
Symplectic	0.48 – 0.50	0.48 – 0.51	0.48 – 0.51	0.52 – 0.56	0.45 – 0.48	0.37 – 0.40
Mixed	0.54 – 0.59	0.46 – 0.50	0.47 – 0.53	0.65 – 0.70	0.44 – 0.48	0.49 – 0.53
Dissipative	0.64 – 0.74	0.65 – 0.69	0.59 – 0.64	0.67 – 0.76	0.63 – 0.69	0.64 – 0.69

TABLE 1. Radii of the annular regions that encompasses most of the poles of the Padé and log-Padé approximants for different frequency vectors. The approximants were computed using Lindstedt series of order at least $N = 128$. Map (6)-(7) with $\gamma = 0.01$. Dissipative: $\lambda_1 = 0.8$, $\lambda_2 = 0.7$. Mixed: $\lambda_1 = 1$, $\lambda_2 = 0.8$. Symplectic: $\lambda_1 = 1$, $\lambda_2 = 1$.

the lower right panel shows the radius of convergence of the Lindstedt coefficients. Given that the poles of the Padé approximants often lie on an irregular curve, we provide an inner and outer circle to confine the regions where most of the poles are located; due to the asymptotic character of the Lindstedt series, we expect that the radius of convergence of the Lindstedt series occurs within the two level lines corresponding to the radii of the inner and outer circles as shown in Figure 4, lower right panel.

We studied also the other frequency vectors introduced in (9), providing an estimate of the breakdown threshold by looking at the intersection of the poles of the Padé approximants with the real axis. The results of such thresholds are summarized in Table 1; also in this case, we provide results in the form of an interval giving the radii of the annular regions containing most of the poles. Table 1 shows that the mean values of the intervals often tend to increase, as the 4D map switches from symplectic to mixed to dissipative.

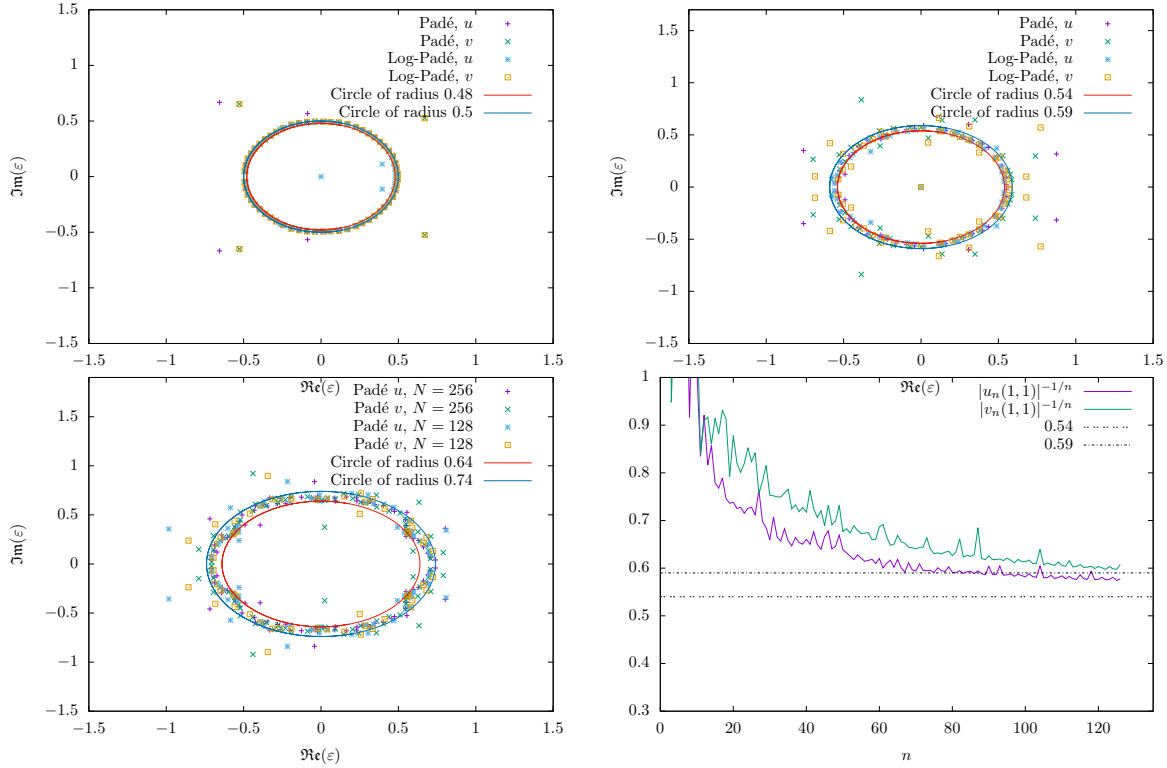


FIGURE 4. Map (6) with $\lambda_1 = \lambda_2 = 1$ (upper left), $\lambda_1 = 1, \lambda_2 = 0.8$ (upper right), $\lambda_1 = 0.8, \lambda_2 = 0.7$ (lower left) for $\underline{\omega}_s, \gamma = 0.01$. The plots display the poles of the Padé and log-Padé approximants for $N = 128$ or (lower left) the poles of the Padé approximants for $N = 128$ and $N = 256$. The lower right panel shows the plots for the estimate of the radius of convergence of the Lindstedt series using coefficients up to order $N = 128$ and $\underline{\psi} = (1, 1)$ for $\lambda_1 = 1, \lambda_2 = 0.8$.

Furthermore, we provide in Table 2 some results concerning the dependence of the thresholds on the coupling parameter. Precisely, we consider the frequency $\underline{\omega}_s$ and we vary the coupling parameter γ on a set of values from 10^{-4} to 0.5. We provide the breakdown threshold again as an interval computed by looking at the poles of the Padé and log-Padé approximants, further validated by the computation of the radius of convergence of the Lindstedt coefficients. As it is expected, the values decrease as the coupling parameter increases.

We conclude by mentioning some results for potentials with two harmonics and a coupling, say $V_{1hc}(x, z) = \sin(x) + \frac{1}{3} \sin(3x) + \gamma \sin(x - z)$, $V_{2hc}(x, z) = \sin(z) + \frac{1}{3} \sin(3z) - \gamma \sin(x - z)$. The plots of Figure 5 show the results for the map (6) in the symplectic case with frequency $\underline{\omega}_s$ and $\gamma = 0.01$. The poles of the Padé and log-Padé approximants are computed up to the order $N = 85$ with a precision of at least 50 digits. The estimate

γ	Symplectic	Mixed	Dissipative
0.0001	0.57 – 0.64	0.57 – 0.71	0.64 – 0.78
0.0005	0.56 – 0.62	0.56 – 0.68	0.64 – 0.78
0.001	0.56 – 0.58	0.56 – 0.64	0.64 – 0.78
0.005	0.50 – 0.52	0.55 – 0.59	0.64 – 0.74
0.01	0.48 – 0.50	0.54 – 0.59	0.64 – 0.73
0.05	0.43 – 0.45	0.45 – 0.52	0.61 – 0.66
0.1	0.40 – 0.43	0.40 – 0.50	0.57 – 0.63
0.25	0.32 – 0.38	0.33 – 0.40	0.46 – 0.54
0.5	0.21 – 0.29	0.26 – 0.31	0.35 – 0.44

TABLE 2. Radii of the annular regions that encompasses most of the poles of the Padé and log-Padé approximants for the map (6)-(7), the frequency $\underline{\omega}_s$ and for different values of the coupling parameter γ . The approximants were computed using Lindstedt series of order at least $N = 128$. Dissipative: $\lambda_1 = 0.8, \lambda_2 = 0.7$. Mixed: $\lambda_1 = 1, \lambda_2 = 0.8$. Symplectic: $\lambda_1 = 1, \lambda_2 = 1$.

of the breakdown threshold is definitely complicated by the very irregular behaviour of the poles that appears in the two-harmonic potential.

7. NEWTON METHOD AND SOBOLEV CRITERION

This Section is devoted to the presentation of Newton method for the 2D (Section 7.1) and 4D cases (Section 7.2); we also describe the Sobolev criterion in 4D (Section 7.3, see [13] for the Sobolev criterion in 2D) to find the breakdown threshold and we provide some results for the 2D (Section 7.4) and 4D maps (Section 7.5).

7.1. Newton method for 2D maps. For the dissipative 2D standard map (5), we use a Newton method that has been implemented very successfully in [13]. It consists in finding a hull function $\underline{P} : \mathbb{T} \rightarrow \mathbb{R}$ and a drift parameter $\mu \in \mathbb{R}$ satisfying equation (13). The details about the construction and implementation of the Newton method in the 2D case can be found in [13].

7.2. Newton method for 4D maps. In the 4D case, we present a procedure borrowed from [14] to find, through a Newton method, the parameterization of an invariant torus. In the following lines we give a brief description of the construction of the corrections at each step of the Newton method.

Consider the map $\underline{f}_{-\mu} : \mathbb{T}^2 \times \mathbb{R}^2 \rightarrow \mathbb{T}^2 \times \mathbb{R}^2$ given by (6). In this Section, we limit to consider a family of conformally symplectic maps $\underline{f}_{-\mu}$ with conformal factor λ equal

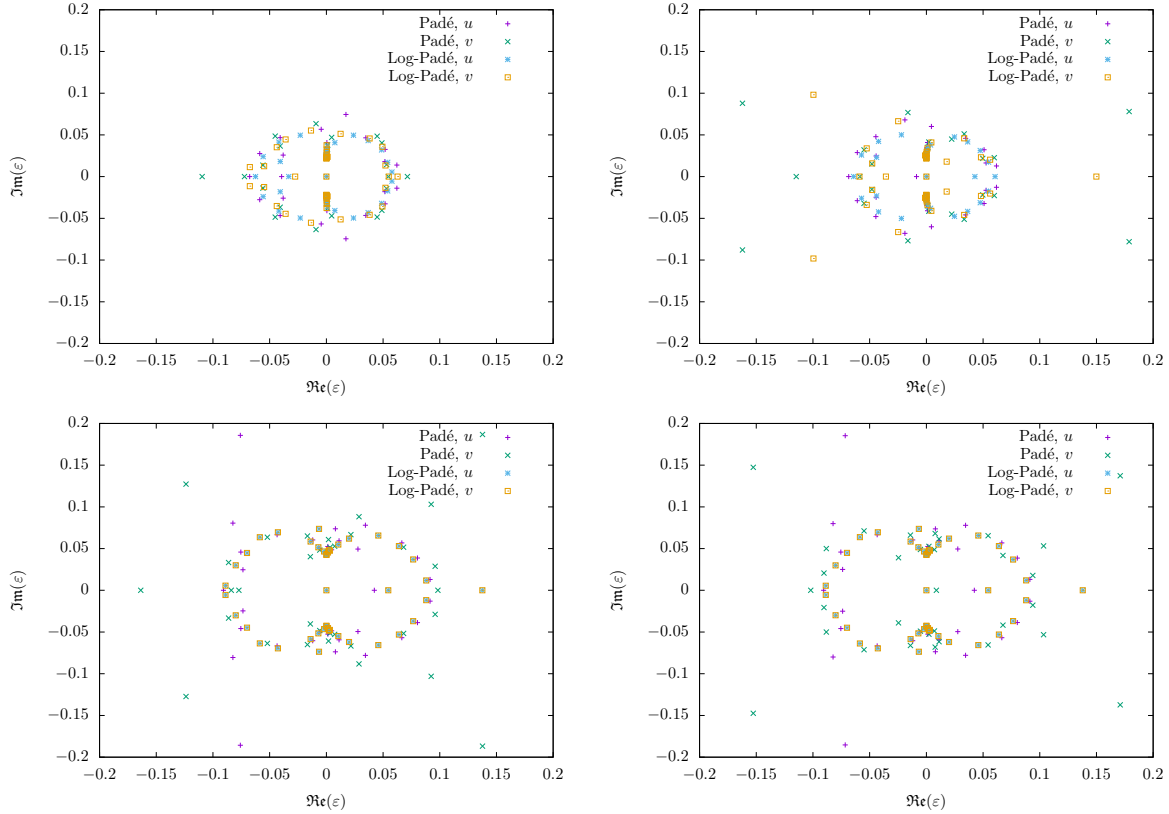


FIGURE 5. Map (6) with the 2-harmonic potential $V_{1hc}(x, z) = \sin(x) + \frac{1}{3} \sin(3x) + \gamma \sin(x - z)$, $V_{2hc}(x, z) = \sin(z) + \frac{1}{3} \sin(3z) - \gamma \sin(x - z)$, $\underline{\omega}_s$, $\gamma = 0.01$. Poles of Padé and log-Padé approximants using Lindstedt series of order $N = 85$. Upper left panel: $\lambda_1 = 1$, $\lambda_2 = 1$. Upper right panel: $\lambda_1 = 1$, $\lambda_2 = 0.8$. Lower left panel: $\lambda_1 = 0.8$, $\lambda_2 = 0.8$. Lower right panel: $\lambda_1 = 0.8$, $\lambda_2 = 0.7$.

for both components y and w . We remark that the extension to the case of different conformal factors, say λ_1, λ_2 , cannot be directly derived from [14], but one could rather use one of the many algorithms implemented and run in [22].

We look for a parameterization $\underline{K} : \mathbb{T}^2 \longrightarrow \mathbb{T}^2 \times \mathbb{R}^2$ and a constant vector $\underline{\mu} \in \mathbb{R}^2$ satisfying the invariance equation (10). Note that if such \underline{K} and $\underline{\mu}$ satisfying (10) exist, then there exists an invariant torus, parameterized by \underline{K} , whose dynamics is conjugated to a rotation by $\underline{\omega}$. Notice also that \underline{K} needs to satisfy a normalization condition, due to the fact that the solution of (10) is not unique ([14]).

The Newton method we use takes advantage of the so-called “automatic reducibility”: in a neighborhood of an invariant torus there exists an explicit change of coordinates that makes the linearization of the invariance equation (10) into an equation with constant

coefficients (see equation (31) below). That is, defining $M(\underline{\theta})$ as the 4×4 matrix

$$M(\underline{\theta}) = [D\underline{K}(\underline{\theta})|J^{-1}D\underline{K}(\underline{\theta})N(\underline{\theta})] , \quad (27)$$

where $N(\underline{\theta}) = [D\underline{K}(\underline{\theta})^\top D\underline{K}(\underline{\theta})]^{-1}$, then, if \underline{K} and $\underline{\mu}$ satisfy (10), one has that

$$Df_{\underline{\mu}} \circ \underline{K}(\underline{\theta})M(\underline{\theta}) = M(\underline{\theta} + 2\pi\underline{\omega}) \begin{pmatrix} Id & S(\underline{\theta}) \\ 0 & \lambda Id \end{pmatrix} , \quad (28)$$

where $S(\underline{\theta})$ is an explicit function depending on $D\underline{K}(\underline{\theta})$ and $Df_{\underline{\mu}} \circ \underline{K}(\underline{\theta})$ (see [14] for the explicit formulation of the function S).

Next, we briefly describe the quasi-Newton method used to find solutions of (10); a detailed exposition of such method can be found in [14]. We start with an approximate solution of (10), say

$$f_{\underline{\mu}} \circ \underline{K} - \underline{K} \circ T_{\underline{\omega}} = \underline{E} ,$$

where $T_{\underline{\omega}}(\underline{\psi}) = \underline{\psi} + 2\pi\underline{\omega}$ and the error \underline{E} in the approximation is supposed to be small. The Newton method introduced in [14] consists in finding corrections $\underline{\Delta}$ and $\underline{\sigma}$ to \underline{K} and $\underline{\mu}$, respectively, such that the approximate solution of (10) associated to $\underline{K} + \underline{\Delta}$, $\underline{\mu} + \underline{\sigma}$ quadratically reduces the error. Taking into account that

$$f_{\underline{\mu}+\underline{\sigma}} \circ (\underline{K} + \underline{\Delta}) = f_{\underline{\mu}} \circ \underline{K} + [Df_{\underline{\mu}} \circ \underline{K}]\underline{\Delta} + [D_{\underline{\mu}}f_{\underline{\mu}} \circ \underline{K}]\underline{\sigma} + O(\|\underline{\Delta}\|^2) + O(\|\underline{\sigma}\|^2) ,$$

the Newton method consists in finding $\underline{\Delta}$ and $\underline{\sigma}$ satisfying

$$[Df_{\underline{\mu}} \circ \underline{K}]\underline{\Delta} - \underline{\Delta} \circ T_{\underline{\omega}} + [D_{\underline{\mu}}f_{\underline{\mu}} \circ \underline{K}]\underline{\sigma} = -\underline{E} . \quad (29)$$

Instead of solving (29), the main idea in [14] is to use the automatic reducibility to find an approximate solution of (13), that still leads to a quadratically convergent procedure. Using the matrix M defined in (27), a change of variables is introduced by setting

$$\underline{\Delta} = M\underline{W} .$$

In the new unknowns \underline{W} and $\underline{\sigma}$, equation (29) transforms into

$$[Df_{\underline{\mu}} \circ \underline{K}]M\underline{W} - (M \circ T_{\underline{\omega}})(\underline{W} \circ T_{\underline{\omega}}) + [D_{\underline{\mu}}f_{\underline{\mu}} \circ \underline{K}]\underline{\sigma} = -\underline{E} .$$

Then using (28), and ignoring an error term in (28) coming from the fact that \underline{K} , $\underline{\mu}$ is an approximate solution to (10), one obtains

$$M \circ T_{\underline{\omega}} \left[\begin{pmatrix} Id & S(\underline{\theta}) \\ 0 & \lambda Id \end{pmatrix} \underline{W} - \underline{W} \circ T_{\underline{\omega}} \right] + [D_{\underline{\mu}}f_{\underline{\mu}} \circ \underline{K}]\underline{\sigma} = -\underline{E} . \quad (30)$$

As it is noted in [14], equation (30) reduces to difference equations with constant coefficients, so that it can be solved efficiently by using Fourier methods. Using the notation

$\underline{W} = (W_1, W_2)^\top$, $\tilde{\underline{E}} = (M^{-1} \circ T_{\underline{\omega}})\underline{E} := (\tilde{\underline{E}}_1, \tilde{\underline{E}}_2)^\top$, and $\tilde{A} = (M^{-1} \circ T_{\underline{\omega}})D_{\underline{\mu}}f_{\underline{\mu}} \circ \underline{K} := [\tilde{A}_1 | \tilde{A}_2]$, equation (30) can be expressed in components as

$$\begin{aligned} \underline{W}_1 - \underline{W}_1 \circ T_{\underline{\omega}} &= -S\underline{W}_2 - \tilde{\underline{E}}_1 - (\tilde{A}\underline{\sigma})_1 \\ \lambda\underline{W}_2 - \underline{W}_2 \circ T_{\underline{\omega}} &= -\tilde{\underline{E}}_2 - (\tilde{A}\underline{\sigma})_2 . \end{aligned} \quad (31)$$

The system of equations (31) has an upper triangular structure and the way to solve it is summarized in Algorithm 10 described in Appendix C.

Implementing the Newton method to find approximations of \underline{K} , $\underline{\mu}$, and computing suitable norms of such approximations will allow us to get information on the breakdown threshold of invariant attractors (see Section 7.3). The algorithm to implement one step of the Newton method, thoroughly explained in [14] (see Appendix C for the sake of completeness), is very efficient, since all steps involve only diagonal operations in the Fourier space and/or diagonal operations in the real space. Moreover, if we represent a function in discrete points or in Fourier space, we can compute the other functions through a FFT; using N Fourier modes to discretize the function, then we need only $O(N)$ storage and $O(N \log N)$ arithmetic operations.

7.3. Sobolev criterion for the 4D case. Given a periodic function f on \mathbb{T}^2 , we consider a sample of points on a regular grid of size $\underline{L} = (L_1, L_2)$ as

$$\underline{\psi}_j := (\psi_{j_1}, \psi_{j_2}) = \left(\frac{2\pi j_1}{L_1}, \frac{2\pi j_2}{L_2} \right),$$

where $\underline{j} = (j_1, j_2) \in \mathbb{Z}^2$ and $0 \leq j_1 < L_1$, $0 \leq j_2 < L_2$. The total number of points is given by $L_D = L_1 L_2$. To implement numerically the Newton step described in Section 7.2, we consider the Fourier series expansion of $f(\underline{\psi}) = \sum_{\underline{k}'} \hat{f}_{\underline{k}'} e^{i\underline{k}' \cdot \underline{\psi}}$ with the multi-index $\underline{k}' = (k'_1, k'_2)$ given as follows:

$$k'_l = \begin{cases} k_l & \text{if } 0 \leq k_l \leq L_l/2 \\ k_l - L_l & \text{if } L_l/2 < k_l < L_l \end{cases} .$$

Note that the truncated Fourier series coincides with the Discrete Fourier Transform on the points of the grid. Following [34], we also introduce the tail in the l -th angle ψ_l with $l = 1, 2$ of the truncated Fourier series as follows:

$$\text{tail}_l(\{\hat{f}_{\underline{k}}\}) := \sum_{\mathcal{C}_l} |\hat{f}_{\underline{k}}|, \quad l = 1, 2 ,$$

where \mathcal{C}_l is defined as the set of multi-indices

$$\mathcal{C}_l = \left\{ \underline{k} = (k_1, k_2) : \frac{L_l}{4} \leq k_l \leq \frac{3L_l}{4} \right\} .$$

To control the quality of the approximation we ask this tail to be small.

The rigorous results described in [14] and [19] provide an algorithm to approximate the analyticity breakdown. Given a well-behaved approximate solution to (13), there are true solutions in a neighborhood and, moreover, close to the breakdown the Sobolev semi-norms of high enough order must blow up. For a function $f : \mathbb{T}^2 \rightarrow \mathbb{R}$, we introduce the L^2 -norm as $\|f\|_{L^2} := (\sum_{\underline{k} \in \mathbb{Z}^2} |\hat{f}_{\underline{k}}|^2)^{1/2}$. Then, following [7], we define the semi-norms

$$\|f\|_{r,\parallel} := \|(2\pi\underline{\omega} \cdot \nabla)^r f\|_{L^2}, \quad \|f\|_{r,\perp} := \|(2\pi\underline{\omega}^\perp \cdot \nabla)^r f\|_{L^2},$$

where $\underline{\omega} = (\omega_1, \omega_2)$ and $\underline{\omega}^\perp = (-\omega_2, \omega_1)$. These norms provide information about the regularity of the torus on a single direction ($\underline{\omega}$ or $\underline{\omega}^\perp$). The blow up of any of the norms we consider implies the blow up of the Sobolev norm $\|\nabla^r f\|_{L^2}$. We have introduced these semi-norms, because it is easier to compute them numerically and because they also provide information of the directions in which the derivatives blow up faster. For trigonometric polynomials, say $f^{(N)}(\underline{\psi}) = \sum_{|\underline{k}| \leq N} \hat{f}_{\underline{k}} e^{i\underline{k} \cdot \underline{\psi}}$, the semi-norms are computed as follows:

$$\|f^{(N)}\|_{r,\parallel} = \left(\sum_{|\underline{k}| \leq N} (2\pi\underline{\omega} \cdot \underline{k})^{2r} |\hat{f}_{\underline{k}}|^2 \right)^{1/2}, \quad \|f^{(N)}\|_{r,\perp} = \left(\sum_{|\underline{k}| \leq N} (2\pi\underline{\omega}^\perp \cdot \underline{k})^{2r} |\hat{f}_{\underline{k}}|^2 \right)^{1/2}.$$

The domain of existence of invariant tori can be computed using an approximate solution $\underline{K}_\varepsilon, \underline{\mu}_\varepsilon$ of equation (10) with $\underline{K}_\varepsilon = (K_1, K_2, K_3, K_4)$ represented by trigonometric polynomials; a regular behavior of the Sobolev norms of $\underline{K}_\varepsilon$, as the parameter ε increases, provides evidence of the existence of the quasi-periodic orbit. The algorithm to identify the boundary of the existence domain can be described as follows:

Algorithm 8. Use $\underline{K}_0, \underline{\mu}_0$ for the integrable case ($\varepsilon = 0$).

Repeat

Increase the parameter ε along the positive real axis

Run the Newton step (Algorithm 10 in Appendix C)

If *iteration of the Newton step does not converge*

decrease the increment in the parameter ε

Else *(Iteration success)*

Record the values of the parameters and compute the semi-norms of the solution

If *for any index l , any of the tails $\text{tail}_l(\{\hat{K}_{\underline{k},i}\})$ exceeds a given value*

Double the number of Fourier coefficients in the l -angle

Until one of the Sobolev seminorms of the approximate solution exceeds a given value

Remark 9. We note that Algorithm 8 is also used for the 2D case. The only change is that there is only one tail for the hull function that solves (13). Also, in this case the Sobolev norm is defined as $\|u\|_r := \|\partial_\theta^r u\|_{L^2}$, and for a trigonometric polynomial $u^{(N)}(\theta) = \sum_{|k| \leq N} \hat{u}_k e^{ik\theta}$ the norm is computed as $\|u^{(N)}\|_r = \left(\sum_{|k| \leq N} k^{2r} |\hat{u}_k|^2 \right)^{1/2}$.

7.4. Results for the 2D case. The results of the implementation of the Newton method and the Sobolev criterion for the 2D case are summarized in Figure 6, which shows the Sobolev norm of the hull function u appearing in (26), providing an estimate of the breakdown threshold which is consistent with the value 0.758 which was found in Figure 2 in the case $\omega = s^{-1}$, $\lambda = 0.8$, $V(x) = \sin x$ (left plot). The estimate of the threshold is consistent with 0.189 for the two harmonics case $V(x) = \sin(x) + \frac{1}{3} \sin(3x)$ (right plot). Additional details for different values of ε on the norm of the hull function and the norm of the error are given in Table 3.

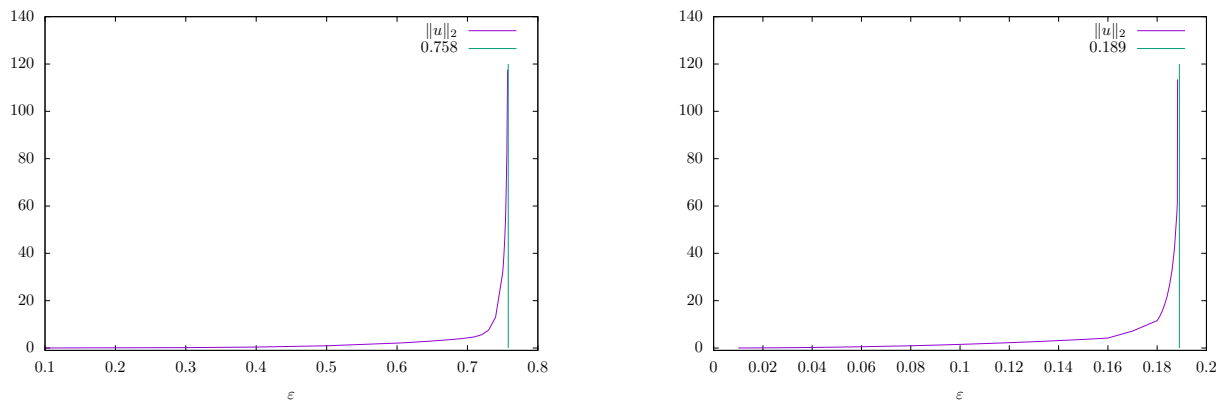


FIGURE 6. Map (5) with $\omega = s^{-1}$, $\lambda = 0.8$, graph of $\|u\|_2$. Left: $V(x) = \sin x$. Right: $V_{2h}(x) = \sin(x) + \frac{1}{3} \sin(3x)$.

7.5. Results for the 4D case. We consider the conformally symplectic case with $\lambda_1 = \lambda_2 = 0.8$. We only monitored the growth of the Sobolev norms for the first two components of the parameterization $K = (K_1, K_2, K_3, K_4)$ with $K_1(\underline{\psi}) = \psi_1 + u(\underline{\psi})$, $K_2(\underline{\psi}) = \psi_2 + v(\underline{\psi})$ as in (12) with $\underline{P} = (u, v)$. The results are presented in Table 4 and Figure 7.

The data included in Table 4 suggest an anisotropic breakdown, a phenomenon that has been observed before in [7]: the derivatives of K blow-up faster in the direction of

TABLE 3. Sobolev norms of the map (5) for different values of the continuation using two different potentials. Parameters: $\omega = s^{-1}$, $\lambda = 0.8$. We have only included the values of ε for which the number of Fourier modes were doubled. L denotes the number of Fourier modes.

$V(x) = \sin(x)$				$V(x) = \sin(x) + \frac{1}{3}\sin(3x)$			
ε	$\ u\ _2$	$\ E\ _\infty$	L	ε	$\ u\ _2$	$\ E\ _\infty$	L
0.1	0.040	8.7e-10	64	0.01	0.018	1.2e-12	64
0.3	0.169	8.0e-15	128	0.02	0.063	2.7e-12	128
0.5	0.968	5.91e-12	256	0.05	0.377	1.6e-11	256
0.6	2.082	8.0e-10	512	0.09	1.235	8.1e-11	512
0.62	2.405	2.4e-13	1024	0.13	2.671	7.2e-11	1024
0.68	3.664	1.4e-12	2048	0.16	4.218	1.5e-13	2048
0.72	5.566	1.0e-10	4096	0.18	11.59	1.5e-10	4096
0.75	31.638	1.6e-10	8192	0.183	18.198	2.1e-13	8192
0.751	35.510	9.1e-13	16384	0.186	32.664	5.2e-11	16384
0.754	54.069	4.3e-12	32768	0.188	56.853	9.7e-10	32768
0.756	82.410	5.5e-11	65536	0.1881	58.969	2.5e-10	65536
0.757	117.512	4.3e-10	131072	0.1882	61.253	2.8e-10	131072
				0.1883	113.47	3.2e-10	262144

$\underline{\omega}$, than they do in the direction of $\underline{\omega}^\perp$. We remark that we stopped the continuation of the Newton method at the last value reported in Table 4, since the computational time was going beyond our computer limits. However, we believe that it is reasonable to expect that the blow-up occurs within the vertical lines at $\varepsilon = 0.64$ and $\varepsilon = 0.71$ shown in Figure 7, left panel, which correspond to the radii of the inner and outer circles of the right panel.

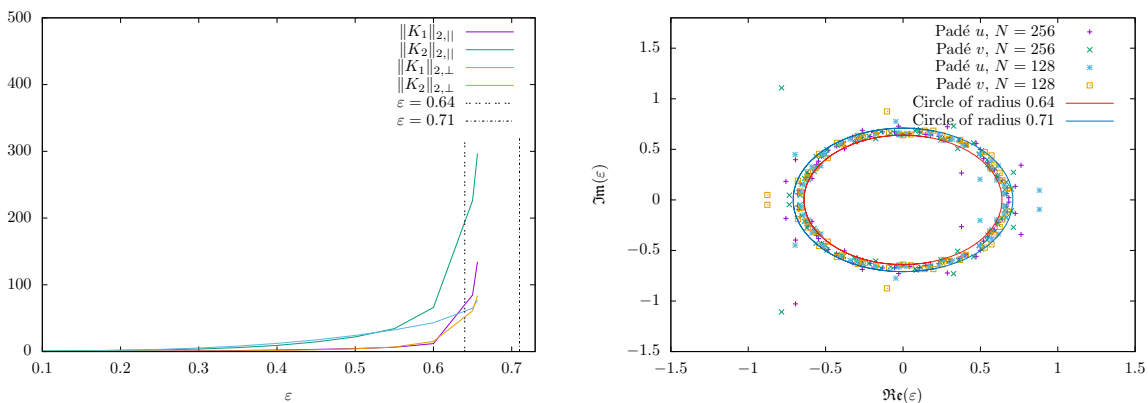


FIGURE 7. Map (6) with $\underline{\omega}_s$, $\lambda_1 = \lambda_2 = 0.8$, $\gamma = 0.01$. Left panel: plots of ε vs $\|K_1\|_{2,\parallel}$, $\|K_2\|_{2,\parallel}$, $\|K_1\|_{2,\perp}$, $\|K_2\|_{2,\perp}$, using the data in Table 4. Right panel: poles of Padé and log-Padé approximants using a Lindstedt series at orders $N = 128$ and $N = 256$.

TABLE 4. $\lambda_1 = \lambda_2 = 0.8$, $\gamma = 0.01$, $\underline{\omega}_s$. Values of the Sobolev norms of the first two components of the approximate solution $K = (K_1, K_2, K_3, K_4)$. The iteration is successful in the Algorithm when the error of the approximation is $< 10^{-9}$. The number of Fourier coefficients in the l -angle is doubled when $\text{tail}_l < 10^{-13}$. L_l denotes the number of Fourier modes used in the angle l .

ε	$\ K_1\ _{2,\parallel}$	$\ K_2\ _{2,\parallel}$	$\ K_1\ _{2,\perp}$	$\ K_2\ _{2,\perp}$	L_1	L_2	$\ E\ _\infty$
0.05	0.056	0.453	0.304	0.083	32	32	3.3e-12
0.10	0.117	0.907	0.635	0.168	64	64	5.1e-12
0.15	0.204	1.371	1.107	0.254	64	64	8.6e-12
0.20	0.355	1.890	1.921	0.351	64	128	1.6e-11
0.25	0.607	2.608	3.281	0.485	128	128	6.2e-11
0.30	0.991	3.815	5.360	0.709	128	128	1.8e-10
0.35	1.538	5.901	8.314	1.097	128	128	5.3e-10
0.40	2.278	9.285	12.311	1.726	256	256	1.1e-16
0.45	3.247	14.433	17.537	2.687	256	256	1.1e-15
0.50	4.505	22.041	24.203	4.142	256	256	1.5e-14
0.55	6.396	34.398	32.564	6.813	512	512	5.2e-14
0.60	11.866	66.153	43.077	15.186	512	512	6.5e-10
0.65	84.682	226.140	64.864	60.968	1024	1024	2.2e-12
0.65625	134.608	296.754	76.873	83.737	1024	2048	7.5e-13

8. APPROXIMATION OF THE TORI THROUGH PERIODIC ORBITS

In this Section, we compute the periodic orbits approximating the tori with irrational frequency. In fact, the well-known numerical method developed by J. Greene in [32] for the determination of the stochastic transition of invariant tori is based on the conjecture that the tori breakdown when the periodic orbits, with frequency equal to the rational approximants to the frequency of the torus, change from stability to instability. Greene method was originally developed for the symplectic standard map and later used for other models, including the 2D dissipative standard map in [13]. The application of an extension of Greene method to dissipative systems is made difficult by the fact that periodic orbits exist for a whole interval of the parameters, the so-called *Arnold tongues* ([3]). Moreover, in the conservative case in 2D one can take advantage of the existence of symmetry lines to ease the search of periodic orbits; instead, symmetry lines do not exist in the dissipative case (and they were not needed for the computation of the Padé approximants or the Sobolev norms); in the 4D case, even if they exist, it is required to implement two dimensional zero finders. Furthermore, the application of the extension of Greene method to higher dimensional systems (like the 4D standard map) is not trivial,

since the search for the approximating periodic orbits might be computationally difficult, as shown for example in [21].

In the rest of this Section, we recall some results on Greene method for dissipative systems (Section 8.1) and we implement a numerical method with the aim to apply an extension of Greene method (Sections 8.2 and 8.3).

8.1. An extension of Greene method for dissipative systems. A method for computing the breakdown threshold of quasi-periodic solutions was presented in [32] for the 2D symplectic standard map, satisfying the twist condition. Greene method is based on the assertion that the invariant circle exists if and only if the approximating periodic orbits are at the boundary of linear stability. A partial justification in the symplectic case was presented in [29], [39], which showed that when the invariant torus exists, one can obtain bounds on a quantity called *residue*, which is a measure of stability of the approximating periodic orbits. A Greene-like method has been applied in [13] to the dissipative standard map, while [20] extends the method to conformally symplectic and dissipative systems in any dimension, and provides a partial justification. The difference with the symplectic case is that the conformally symplectic systems need adjusting parameters and moreover they do not admit Birkhoff invariants. The results in [20] show that if the rotational torus exists, one can predict the eigenvalues of the approximating periodic orbits for values of the parameters close to that of the torus; it gives also results on Arnold tongues. Two proofs are given, the first one based on deformation theory and the second one combining the theory of normally hyperbolic invariant manifolds with averaging theory. A property of conformally symplectic systems is the *pairing rule*, which states that the eigenvalues of a d -dimensional conformally symplectic matrix with conformal factor λ are paired; precisely, if χ_i , $i = 1, \dots, d$, is an eigenvalue, then $\lambda\chi_i^{-1}$ is also an eigenvalue. The second proof of [20] using the theory of normally hyperbolic invariant manifolds applies to general systems with a normally hyperbolic rotational circle and concludes that the periodic orbits have d eigenvalues close to 1. When the system is conformally symplectic, using the pairing rule, we recover the same result as before. We stress that the result could apply also to the mixed systems discussed here, but we have not pursued the implementation.

An extension of the residue to conformally symplectic systems in any dimension can be given in terms of the distance of the spectrum of a periodic orbit with period q to the set $\{1, \lambda^q\}$, which represents the spectrum of the periodic orbit when the map is integrable.

According to [20], let us denote by

$$c(x) := x^{2d} + c_{2d-1}x^{2d-1} \dots + c_1x + \lambda^{dq}, \quad c_j \in \mathbb{R},$$

the characteristic polynomial of the derivative of the map over the full cycle of the periodic orbit with period q . The coefficients c_j are parameterized by the spectral numbers χ_j . Consider the space $\mathcal{M}_0 = \mathbb{T}^d \times B$ with $B \subset \mathbb{R}^d$ a ball around zero, endowed with the standard symplectic form $\Omega_0 = \sum_{j=1}^d dy_j \wedge dx_j$, where $\underline{x} \in \mathbb{T}^d$, $\underline{y} \in B$; let f_0 be the conformal symplectic map with respect to Ω_0 defined as

$$f_0(\underline{y}, \underline{x}) = (\lambda \underline{y}, \underline{x} + \underline{\omega})$$

with $\underline{\omega}$ Diophantine. Then, the characteristic polynomial associated to f_0 is given by

$$(x-1)^d(x-\lambda^q)^d := x^{2d} + c_{2d-1}^0 x^{2d-1} + \dots + c_1^0 x + \lambda^{dq}, \quad c_j^0 \in \mathbb{R}.$$

Finally, the residue R can be defined as the distance between the coefficients of the characteristic polynomials:

$$R := \sum_{j=1}^d |c_j - c_j^0|. \quad (32)$$

We will try to construct the approximating periodic orbits also in the dissipative 4D case with different conformal factors to verify at least numerically whether their linear stability provides information on the breakdown threshold of the torus (see Section 8.3). The implementation of the method in the 4D case is the following. We fix a rational approximant to the frequency of the torus. For each approximant and for a fixed value of ε , we compute a corresponding periodic orbit within the associated Arnold tongue. In principle, we should take the supremum of the residue over all the periodic orbits within the Arnold tongue and we should take periodic orbits far from the boundaries of the tongue. However, this goes beyond our computational capabilities and we are limited to select one periodic orbit as far as possible from the boundaries of the tongue. Then, we compute the residue as a function of ε ; when the residue is regular, there is evidence of the stability of the periodic orbits and hence of the existence of the torus ([20]).

8.2. Periodic orbit approximants in the 2D case. We show two examples of stable periodic orbits in Figure 8 for the 2D dissipative standard map with $\lambda = 0.8$; the left panel refers to the approximant $610/987$ to ϖ and the right panel refers to the approximant $619/820$ to s^{-1} .

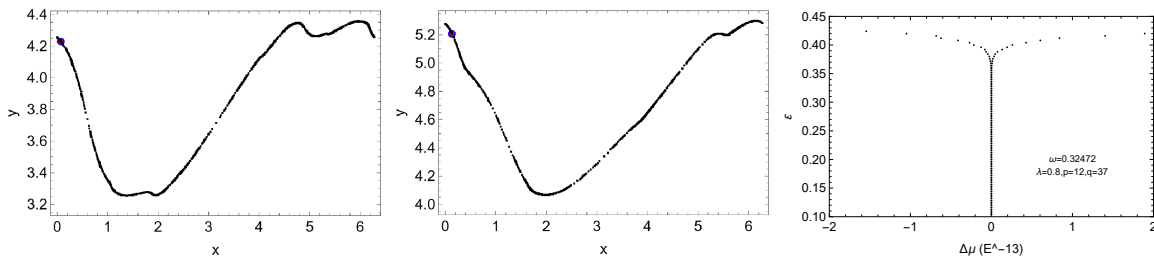


FIGURE 8. 2D map (5) with $V(x) = \sin x$, $\lambda = 0.8$. Stable periodic orbits with $\omega_1 = 610/987$, $\varepsilon = 0.973$ (left) and $\omega_1 = 619/820$, $\varepsilon = 0.758$ (middle); we start the iteration of the map from the red point. In the right panel we show a numerical approximation of the Arnold tongue for $\omega = s^{-1}$, $\lambda = 0.8$, $(p, q) = (12, 37)$.

TABLE 5. Critical parameter and drift for stable periodic orbits of the map (5) with $\lambda = 0.8$, approximating to the frequencies $\omega_1 = \varpi$ (left) and $\omega_1 = s^{-1}$ (right).

p	q	ε_c	μ	p	q	ε_c	μ
2	3	1.384	0.82796	3	4	1.156	0.924791
3	5	1.185	0.75105	37	49	0.787	0.935855
5	8	1.123	0.78265	40	53	0.779	0.935884
8	13	1.028	0.76804	77	102	0.774	0.935981
13	21	1.004	0.77153	271	359	0.753	0.936199
21	34	0.992	0.77043	619	820	0.758	0.936139
34	55	0.984	0.77090				
55	89	0.970	0.77090				
89	44	0.946	0.77121				
144	233	0.945	0.77119				
233	377	0.975	0.77088				
377	610	0.976	0.77086				
610	987	0.973	0.77089				

It is known that in the dissipative case the periodic orbits can be found within an interval of the drift parameter, the Arnold tongue; an example of a numerical approximation is given in Figure 8, right panel. As shown in [4] and [46], the width of the Arnold tongue scales as ε^q , where q is the period of the periodic orbit.

The results of the extension of Greene method for ϖ and s^{-1} are presented in Table 5, which shows the drift μ and the maximum values of the critical parameter ε_c for which the periodic orbit with frequency p/q given by the rational approximants to the irrational frequency is stable. The values $\varepsilon_c = 0.973$ for ϖ and $\varepsilon_c = 0.758$ for s^{-1} are consistent with the values shown in Figure 1 and 2 (upper right plot) based on the computation

of the poles of Padé approximants as well as with the results for s^{-1} given in Section 7 using Sobolev criterion.

8.3. Periodic orbit approximants in the 4D case. Let us denote by $\underline{f} : \mathbb{R}^2 \times \mathbb{T}^2 \rightarrow \mathbb{R}^2 \times \mathbb{T}^2$ the map (6) with the potential in (7). Let $\tilde{\underline{f}} : \mathbb{R}^4 \rightarrow \mathbb{R}^4$ be the lift of \underline{f} and let $\underline{\omega}_p = (p_1/q, p_2/q)$ be a frequency vector with $p_1, p_2 \in \mathbb{Z}$, $q \in \mathbb{Z} \setminus \{0\}$. A periodic orbit with frequency $\underline{\omega}_p$ satisfies the condition

$$\tilde{\underline{f}}^q(\underline{X}) = \underline{X} + (0, 2\pi p_1, 0, 2\pi p_2)$$

for $\underline{X} = (y, x, w, z)$. Searching for periodic orbits is equivalent to finding the roots of the function

$$\underline{G}(\underline{X}) := \tilde{\underline{f}}^q(\underline{X}) - \underline{X} - (0, 2\pi p_1, 0, 2\pi p_2) . \quad (33)$$

We recall that the frequency can be computed as in Remark 3. A heuristic method for finding periodic orbits is presented in Appendix D; we stress that the method is just based on experimental evidence and on an a-posteriori corroboration that we effectively found the desired periodic orbits. Unfortunately we are not aware of more efficient (and possibly rigorously justified) methods to find periodic orbits in the non-symplectic 4D case including drifts.

The linear stability of the periodic orbits is calculated by computing the eigenvalues κ_1, κ_2 of the product of the Jacobian of the map over the periodic orbit. If $\max(|\kappa_1|, |\kappa_2|) > 1$ the orbit is said to be unstable. An example of the computation of the linear stability for some approximants to $\underline{\omega}_s$ is given in Table 6 in the dissipative case with $\lambda_1 = 0.8$, $\lambda_2 = 0.7$; the convergence to a limit value is not evident and possibly larger approximants would be needed.

The evidence of the existence of the Arnold tongues in 4D (see [20]) is obtained by taking a reference value of the drifts and initial conditions for a given periodic orbit, having fixed the perturbing, coupling and dissipative parameters, and then by taking nearby random values of the drifts and initial conditions, which are used as initial guess of the root finding method to find another periodic orbit of the same period. An example is given in Figure 9 for the periodic orbit with $p_1 = 3$, $p_2 = 7$, $q = 9$ (one of the first approximants to $\underline{\omega}_s$). We analyzed the conformally symplectic 4D map with $\lambda_1 = \lambda_2 = 0.8$ and the coupling parameter equal to $\gamma = 0.01$. The graphs show the regions (and a zoom) of the drifts μ_1, μ_2 as a function of the perturbing parameter ε , delimited by the blue and red dots in which one can find a periodic orbit; as in the 2D case, the results

TABLE 6. Parameters and initial conditions for the periodic orbits approximating $\underline{\omega}_s$ with frequency $\underline{\omega} = (p_1/q, p_2/q)$ for $\gamma = 0.01$, $\lambda_1 = 0.8$, $\lambda_2 = 0.7$. The values of ε are those for which the orbits are still linearly stable and just before they become unstable.

	p_1	p_2	q	ε	y	x	w	z	μ_1	μ_2
1	1	2	3	0.152	2.1414	3.0828	4.240	0.069	0.4191	0.8374
2	3	7	9	0.934	2.3460	3.0916	4.330	3.230	0.4238	0.9463
3	12	28	37	0.516	1.8524	6.2093	5.050	0.128	0.4097	0.9427
4	37	86	114	0.541	1.8433	6.2090	5.050	0.126	0.4098	0.9395
5	151	351	465	0.704	1.7718	6.2057	4.390	3.220	0.4078	0.9367
6	465	1081	1432	0.639	1.7992	6.2083	5.120	0.131	0.4090	0.9378

are consistent with the qualitative and theoretical results given in [4] and [46]. Figure 9 shows also a 3D picture of the Arnold tongue (lower left panel).

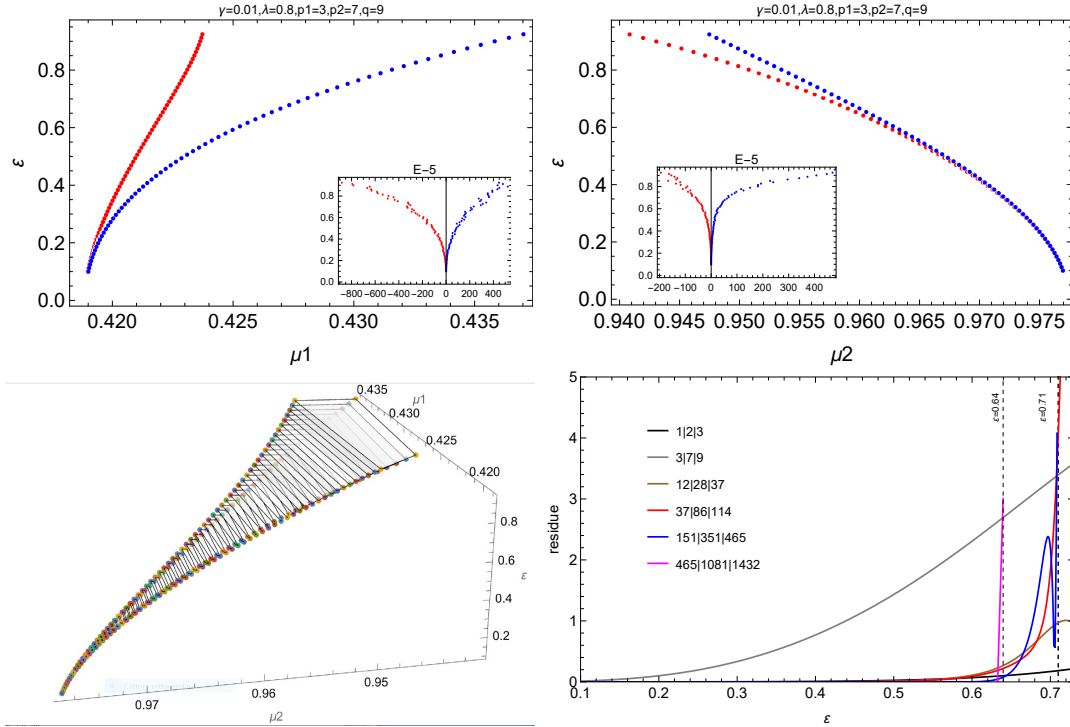


FIGURE 9. Map (6)-(7) with $\lambda_1 = \lambda_2 = 0.8$, $\gamma = 0.01$. Regions of the drifts μ_1 (upper left), μ_2 (upper right), μ_1 and μ_2 (lower left) versus ε for $p_1 = 3$, $p_2 = 7$, $q = 9$. The red and blue dots give the region within which one can find a periodic orbit. Residues of the first few approximants to $\underline{\omega}_s$ for increasing values of ε (lower right).

We investigated further the breakdown threshold by computing the residue of the approximating periodic orbits according to the definition given in (32). Within the

numerical ranges found for the Arnold tongues, we tried to select the periodic orbits far from their boundaries. The results for some approximants to $\underline{\omega}_s$ are shown in the lower right panel of Figure 9.

Unfortunately, the implementation of this method does not allow to draw definite conclusions about the breakdown threshold, although we notice a blow-up of the residue within the region found to bound the domain of the Padé approximants of Figure 7.

9. CONCLUSIONS

We have investigated the breakdown of rotational invariant tori in 2D and 4D standard maps, using different formulations: symplectic, conformally symplectic, mixed, dissipative maps. We have implemented three different methods: *(i)* the computation of the Lindstedt series expansions, *(ii)* the construction of invariant tori through a Newton method, *(iii)* the approximation of the tori through periodic orbits.

The Lindstedt series expansions to a given order allows one to estimate the radius of convergence and the domain of analyticity of the tori through the computation of the Padé approximants in the complex parameter plane. The Newton method allows one to construct an approximation of the parameterization and the drift, whose Sobolev norms provide an indication of the breakdown of the tori when the norms blow up. The construction of the periodic orbits with frequencies approximating that of the invariant torus is at the basis of Greene method, according to which the breakdown of the tori is related to the stability properties of the approximating periodic orbits.

We stress that method *(i)* can be implemented in all maps, method *(ii)* in the formulation given in [14] works only for symplectic and conformally symplectic systems, though [22] provides an extension to the general dissipative case with different conformal factors, method *(iii)* has partial rigorous justifications as shown in [29], [39], [20].

In the 2D cases, all three methods agree to a fairly good degree of accuracy. The domains of analyticity are regular when the potential has only one harmonic and become flower-shaped or irregular when the potential has 2 harmonics. Taking different values of the dissipative parameters, we noticed that often the breakdown thresholds are smaller as we approach the symplectic limit at which branch singularities become more evident ([27], [28]).

In the 4D cases, the implementation of all methods requires a bigger computational effort. Also in this case, we often noticed a decrease of the threshold from dissipative to symplectic, independently of the frequency as shown in Table 1. Besides, the threshold

decreases when the coupling parameter increases, see Table 2. The computation of periodic orbits in the 4D cases becomes particularly difficult, due to the fact that one has a large set of unknowns, given by the four initial conditions and the two drifts. In all non-symplectic cases, one cannot rely on the existence of symmetry lines and one needs to find the periodic orbits in their Arnold tongues, whose structure certainly deserves a deeper investigation. Due to these difficulties, our implementation of an extension of Greene method in higher dimensions was inconclusive.

Acknowledgements. We are grateful to Renato Calleja for useful suggestions. We are deeply indebted with Rafael de la Llave for many discussions, which helped us to improve this work. We also thank the anonymous referee for many comments that greatly contributed to improve the presentation of this work.

APPENDIX A. JACOBI-PERRON ALGORITHM

For a 2D vector $\underline{\omega} = (\omega_1, \omega_2)$, the Jacobi-Perron algorithm (see [43]) allows one to construct the integer sequences $p_{1,i}$, $p_{2,i}$, q_i , such that $(p_{1,i}/q_i, p_{2,i}/q_i)$ are rational approximants to $\underline{\omega}$. For $d = 2$, consider the map

$$T(x, y) = \left(\frac{y}{x} - a_1, \frac{1}{x} - b_1 \right),$$

with

$$a_1 = a_1(x, y) = \left\lfloor \frac{y}{x} \right\rfloor, \quad b_1 = b_1(x, y) = \left\lfloor \frac{1}{x} \right\rfloor,$$

and $a_j(x, y) = a_1(T^{j-1}(x, y))$, $b_j(x, y) = b_1(T^{j-1}(x, y))$. According to [43], the approximants in terms of sequences $p_{1,n}$, $p_{2,n}$, q_n are defined by the matrix product

$$\begin{pmatrix} p_{1,n-2} & p_{1,n-1} & p_{1,n} \\ p_{2,n-2} & p_{2,n-1} & p_{2,n} \\ q_{n-2} & q_{n-1} & q_n \end{pmatrix} = \prod_{j=1}^n \begin{pmatrix} 0 & 0 & 1 \\ 1 & 0 & a_j \\ 0 & 1 & b_j \end{pmatrix}.$$

We notice that

$$\begin{pmatrix} p_{1,n-1} & p_{1,n} & p_{1,n+1} \\ p_{2,n-1} & p_{2,n} & p_{2,n+1} \\ q_{n-1} & q_n & q_{n+1} \end{pmatrix} = \begin{pmatrix} p_{1,n-2} & p_{1,n-1} & p_{1,n} \\ p_{2,n-2} & p_{2,n-1} & p_{2,n} \\ q_{n-2} & q_{n-1} & q_n \end{pmatrix} \begin{pmatrix} 0 & 0 & 1 \\ 1 & 0 & a_{n+1} \\ 0 & 1 & b_{n+1} \end{pmatrix}.$$

Taking only the 3rd column of the matrix product at the $(n + 1)$ -th step, we get the vectorial recursive formula:

$$\begin{pmatrix} p_{1,n+1} \\ p_{2,n+1} \\ q_{n+1} \end{pmatrix} = \begin{pmatrix} p_{1,n-2} \\ p_{2,n-2} \\ q_{n-2} \end{pmatrix} + \begin{pmatrix} p_{1,n-1} \\ p_{2,n-1} \\ q_{n-1} \end{pmatrix} a_{n+1} + \begin{pmatrix} p_{1,n} \\ p_{2,n} \\ q_n \end{pmatrix} b_{n+1}.$$

The recursion can be solved up to order $n > 0$ using the starting values (that leave the matrix product unchanged):

$$\begin{pmatrix} p_{1,-2} & p_{1,-1} & p_{1,0} \\ p_{2,-2} & p_{2,-1} & p_{2,0} \\ q_{-2} & q_{-1} & q_0 \end{pmatrix} = \begin{pmatrix} 1 & 0 & 0 \\ 0 & 1 & 0 \\ 0 & 0 & 1 \end{pmatrix} .$$

APPENDIX B. PADÉ APPROXIMANTS

The analyticity domains of the Lindstedt series expansions of Section 6 can be obtained through the computation of the Padé approximants, that we briefly recall as follows, referring to [5] for further details. Given the series

$$W(\varepsilon) = \sum_{k=1}^{\infty} W_k \varepsilon^k ,$$

we define the Padé approximants to W of order $[M, N]$ for $M, N \in \mathbb{N}$ as the functions $\mathcal{P}_{M,N}(\varepsilon)$, which are the ratio of the polynomials $Q_1^{(M)}(\varepsilon)$, $Q_2^{(N)}(\varepsilon)$ of degree, respectively, M and N , say

$$\mathcal{P}_{M,N}(\varepsilon) := \frac{Q_1^{(M)}(\varepsilon)}{Q_2^{(N)}(\varepsilon)} ,$$

such that the Taylor expansion of $\mathcal{P}_{M,N}(\varepsilon)$ coincides with the Taylor expansion of W up to order $M + N$:

$$W(\varepsilon)Q_2^{(N)}(\varepsilon) - Q_1^{(M)}(\varepsilon) = O(\varepsilon^{M+N+1}) .$$

We can expand $Q_1^{(M)}$ and $Q_2^{(N)}$ as

$$Q_1^{(M)}(\varepsilon) = \sum_{j=0}^M Q_{1,j} \varepsilon^j , \quad Q_2^{(N)}(\varepsilon) = \sum_{j=0}^N Q_{2,j} \varepsilon^j .$$

Then, the function $\mathcal{P}_{M,N}(\varepsilon)$ contains $M + N + 1$ unknown coefficients, since we can normalize $Q_{2,0} = 1$.

The coefficients $Q_{1,j}$, $Q_{2,j}$ can be computed through the following recursive formulae:

$$\begin{aligned} W_i + \sum_{j=1}^N W_{i-j} Q_{2,j} &= 0 , & M < i \leq M + N , \\ W_i + \sum_{j=1}^i W_{i-j} Q_{2,j} &= Q_{1,i} , & 0 \leq i \leq M , \end{aligned}$$

where the first equation gives $Q_{2,j}$ and the second equation gives $Q_{1,j}$.

The analyticity domain of the function W can then be obtained by computing the zeros of $Q_{2,N}$. Typically, one considers diagonal Padé approximants of order $[N, N]$. It

is often necessary to eliminate fake zeros, which can be distinguished from genuine ones for the fact that fake zeros disappear when the order of the Padé approximants changes or when the parameters are slightly changed ([6]).

APPENDIX C. ALGORITHM OF THE NEWTON STEP

In the algorithm below for the Newton step (see [14]), we use the following notation: \overline{B} means the average of B , while $(B)^o$ denotes the zero average part, namely $(B)^o = B - \overline{B}$.

Algorithm 10. *Given $\underline{K} : \mathbb{T}^2 \rightarrow \mathbb{T}^2 \times \mathbb{R}^2$, $\underline{\mu} \in \mathbb{R}^2$, we perform the following computations:*

- 1) $\underline{E} \leftarrow \underline{f}_{\underline{\mu}, \varepsilon} \circ \underline{K} - \underline{K} \circ T_{\underline{\omega}}$
- 2) $\alpha \leftarrow D\underline{K}$
- 3) $N \leftarrow [\alpha^\top \alpha]^{-1}$
- 4) $M \leftarrow [\alpha, J^{-1} \alpha N]$
- 5) $\beta \leftarrow M^{-1} \circ T_{\underline{\omega}}$
- 6) $\tilde{\underline{E}} \leftarrow \beta \underline{E}$
- 7) $P \leftarrow \alpha N$
 $\gamma \leftarrow \alpha^\top J^{-1} \alpha$
 $S \leftarrow (P \circ T_{\underline{\omega}})^\top D \underline{f}_{\underline{\mu}, \varepsilon} \circ \underline{K} J^{-1} P - \lambda (N \circ T_{\underline{\omega}})^\top (\gamma \circ T_{\underline{\omega}}) (N \circ T_{\underline{\omega}})$
 $\tilde{\underline{A}} \leftarrow M^{-1} \circ T_{\underline{\omega}} D \underline{f}_{\underline{\mu}, \varepsilon} \circ \underline{K}$
- 8) $(\underline{Ba})^o$ solves $\lambda(\underline{Ba})^o - (\underline{Ba})^o \circ T_{\underline{\omega}} = -(\tilde{\underline{E}}_2)^o$
 $(\underline{Bb})^o$ solves $\lambda(\underline{Bb})^o - (\underline{Bb})^o \circ T_{\underline{\omega}} = -(\tilde{\underline{A}}_2)^o$
- 9) Find $\overline{W}_2, \underline{\sigma}$ solving

$$\begin{pmatrix} \overline{S} & \overline{S(\underline{Bb})^o} + \overline{\tilde{\underline{A}}_1} \\ (\lambda - 1)Id & \overline{\tilde{\underline{A}}_2} \end{pmatrix} \begin{pmatrix} \overline{W}_2 \\ \underline{\sigma} \end{pmatrix} = \begin{pmatrix} -\overline{\tilde{\underline{E}}_1} - \overline{S(\underline{Ba})^o} \\ -\overline{\tilde{\underline{E}}_2} \end{pmatrix}$$
- 10) $(\underline{W}_2)^o = (\underline{Ba})^o + (\underline{Bb})^o \underline{\sigma}$
- 11) $\underline{W}_2 = (\underline{W}_2)^o + \overline{W}_2$
- 12) $(\underline{W}_1)^o$ solves $(\underline{W}_1)^o - (\underline{W}_1)^o \circ T_{\underline{\omega}} = -(\underline{S}\underline{W}_2)^o - (\tilde{\underline{E}}_1)^o - (\tilde{\underline{A}}_1)^o \underline{\sigma}$
- 13) $\underline{K} \leftarrow \underline{K} + M\underline{W}$
 $\underline{\mu} \leftarrow \underline{\mu} + \underline{\sigma}$.

APPENDIX D. A METHOD TO FIND PERIODIC ORBITS

To solve (33), we proceed as follows. To have an initial guess, we start with the uncoupled 4D case, which splits into a conservative and a dissipative map. We find a

solution for the two uncoupled systems for ε small; in the dissipative case, we compute a periodic orbit within the Arnold tongue. We go back to the 4D coupled case, finding the solution for a given γ not zero and using the solution for $\gamma = 0$ as initial guess. We proceed to find a solution for larger values of ε through a continuation method in ε . A major limitation of this approach is that, within the Arnold tongue, we have not found a unique way to continue a periodic orbit.

To be more specific, we consider the map (6) with the potential in (7) starting with $\gamma = 0$, so that we obtain two uncoupled systems; we first consider the case of a dissipative and a conservative 2D standard map. Denote by $\underline{M}_d : \mathbb{R} \times \mathbb{T} \rightarrow \mathbb{R} \times \mathbb{T}$ the 2D dissipative standard map in the variables (y, x) . For a fixed λ , we look for (y_0, x_0, μ) such that \underline{M}_d admits a periodic orbit with period $2\pi p_1/q$. From (33) with $\gamma = 0$ we need to fulfill the condition

$$(y_0, x_0) = \widetilde{M}_d^q(y_0, x_0; \mu) - (0, 2\pi p_1) , \quad (34)$$

where $\widetilde{M}_d : \mathbb{R}^2 \rightarrow \mathbb{R}^2$ denotes the lift of \underline{M}_d . Since we aim to find three unknowns (y_0, x_0, μ) that solve (34), the system is clearly underdetermined, so we need an additional constraint on the drift parameter. To overcome this problem, we implemented the following procedure, which we have heuristically found and which turns out to be useful for our purposes.

Let us introduce $\mu' \in \mathbb{R}$ as $\mu' = y'(1 - \lambda) - \varepsilon \sin(x')$, which is not constant as (y', x') vary. We define the mapping $\widetilde{M}_e : \mathbb{R}^3 \rightarrow \mathbb{R}^3$ as an extension of \underline{M}_d as follows:

$$\begin{aligned} y' &= \lambda y + \mu + \varepsilon \sin(x) \\ x' &= x + y' \\ \mu' &= y'(1 - \lambda) - \varepsilon \sin(x') . \end{aligned}$$

We are able to find periodic orbits of the extended map, if (y_0, x_0, μ_0) fulfill the following equation

$$(y_0, x_0, \mu_0) = \widetilde{M}_e^q(y_0, x_0, \mu_0) - (0, 2\pi p_1, 0) . \quad (35)$$

Since any triple (y_0, x_0, μ_0) that fulfills (35) also fulfills (34), with $\mu = \mu_0$, we found a $2\pi p_1/q$ periodic orbit of the 2D dissipative map. We notice that the solution of equation (35) will generate two distinct different orbits for the original and extended mappings. Only for $\mu = \mu_0$ we will find the right periodic orbit for the original dissipative map. Since the method is heuristic, we further validate the result by checking that the frequency associated to the solution (y_0, x_0, μ_0) of (34) coincides with the first component of $\underline{\omega}$.

Let us denote the 2D conservative map in the variables (w, z) as $\underline{M}_c : \mathbb{R} \times \mathbb{T} \rightarrow \mathbb{R} \times \mathbb{T}$. To get a periodic orbit with frequency equal to $2\pi p_2/q$, we need to solve

$$(w_0, z_0) = \widetilde{\underline{M}}_c^q(w_0, z_0) - (0, 2\pi p_2) , \quad (36)$$

where we have introduced the lift $\widetilde{\underline{M}}_c : \mathbb{R}^2 \rightarrow \mathbb{R}^2$. The solution of (35) and (36) provides an initial guess for (6) with $\gamma = 0$.

In the 4D case with $\gamma \neq 0$, we proceed as follows. We assume to have a starting point given by $\underline{X}_0 := (y_0, x_0, w_0, z_0)$, so that for $\gamma = 0$ we obtain a periodic orbit for \underline{M}_d with period p_1/q starting from (y_0, x_0) and a periodic orbit for \underline{M}_c with period p_2/q starting from (w_0, z_0) . We apply¹ a continuation method in ε . However, since the solution $\underline{X}^{(\gamma)} = (y^{(\gamma)}, x^{(\gamma)}, w^{(\gamma)}, z^{(\gamma)})$ for $\gamma \neq 0$ requires to adapt (y_0, x_0, μ_0) , as well as (w_0, z_0) simultaneously at each step of the continuation method, we are led to solve the system of equations

$$\begin{aligned} y^{(\gamma)} &= \tilde{f}_1^q(\underline{X}^{(\gamma)}, \mu^{(\gamma)}) & x^{(\gamma)} &= \tilde{f}_2^q(\underline{X}^{(\gamma)}, \mu^{(\gamma)}) - 2\pi p_1 \\ w^{(\gamma)} &= \tilde{f}_3^q(\underline{X}^{(\gamma)}, \mu^{(\gamma)}) & z^{(\gamma)} &= \tilde{f}_4^q(\underline{X}^{(\gamma)}, \mu^{(\gamma)}) - 2\pi p_2 \\ \mu^{(\gamma)} &= \tilde{f}_e^q(\underline{X}^{(\gamma)}, \mu^{(\gamma)}) \end{aligned} \quad (37)$$

with respect to $\underline{X}^{(\gamma)}$ and $\mu^{(\gamma)}$, having defined

$$\tilde{f}_e := y(1 - \lambda) - \varepsilon \frac{\partial}{\partial x} W(x, z; \gamma) .$$

Let us now consider the generalization to the dissipative 4D map with $0 < \lambda_{1,2} \leq 1$, $\mu_{1,2} \in \mathbb{R}$ and W, ε, γ as in (6). Using the same approach outlined for the mixed case, we introduce the extension of the dissipative 4D map through the following additional mapping equations:

$$\mu'_1 = y'(1 - \lambda_1) - \varepsilon \frac{\partial}{\partial x} W(x', z'; \gamma) , \quad \mu'_2 = w'(1 - \lambda_2) - \varepsilon \frac{\partial}{\partial z} W(x', z'; \gamma) .$$

Any periodic orbit of (6) with frequency $(p_1/q, p_2/q)$ needs to fulfill the conditions $y_q^{(\gamma)} = y_0^{(\gamma)}$, $x_q^{(\gamma)} = x_0^{(\gamma)} + 2\pi p_1$, $w_q^{(\gamma)} = w_0^{(\gamma)}$, $z_q^{(\gamma)} = z_0^{(\gamma)} + 2\pi p_2$ with $\mu_{1,q}^{(\gamma)} = \mu_{1,0}^{(\gamma)}$, $\mu_{2,q}^{(\gamma)} = \mu_{2,0}^{(\gamma)}$, where the subindex q means the q -th iterate. Hence, we are led to solve the system of equations (37), replacing the last line with

$$\mu_1^{(\gamma)} = \tilde{f}_{e_1}^q(\underline{X}^{(\gamma)}, \mu_1^{(\gamma)}) , \quad \mu_2^{(\gamma)} = \tilde{f}_{e_2}^q(\underline{X}^{(\gamma)}, \mu_2^{(\gamma)}) \quad (38)$$

¹This procedure is computationally expensive, meaning that: (i) the root finding method might need a large number of iterations to converge to the requested accuracy; (ii) the computations require accuracy, which means even more than 1000 digits in the iteration of the mapping; (iii) if the root finding fails, one needs to find better initial conditions which is highly non trivial and it requires intervention; (iv) the continuation method only works with a small step for the perturbing parameter.

with $(\mu_1, \mu_2) = (\mu_1^{(\gamma)}, \mu_2^{(\gamma)})$, having defined the functions

$$\tilde{f}_{e_1} := y(1 - \lambda_1) - \varepsilon \frac{\partial}{\partial x} W(x, z; \gamma), \quad \tilde{f}_{e_2} := w(1 - \lambda_2) - \varepsilon \frac{\partial}{\partial z} W(x, z; \gamma).$$

We notice that the drift parameters are dynamical variables in the extended mapping. However, their initial values also solve the conditions for periodic orbits of the original mapping (removing the last line in (37)). Thus, the initial values for the drift parameters can also be taken as fixed parameters in the original mapping and provide the correct periodic orbit also in the constant drift system.

REFERENCES

- [1] V. Arnold. Instability of dynamical systems with several degrees of freedom. *Sov. Math. Doklady*, 5:581–585, 1964.
- [2] V. I. Arnol’d. Proof of a theorem of A. N. Kolmogorov on the invariance of quasi-periodic motions under small perturbations. *Russian Math. Surveys*, 18(5):9–36, 1963.
- [3] V. I. Arnol’d. Small denominators. i. mappings of the circumference onto itself. *Amer. Math. Soc. Transl. Ser. 2*, 46:213–284, 1965. English translation: *Amer. Math. Soc. Transl. (2)*, 46:213–284, 1965.
- [4] V. I. Arnold. Remarks on perturbation theory for problems of Mathieu type. *Uspekhi Mat. Nauk*, 38(4(232)):189–203, 1983.
- [5] G. A. Baker, G. A. Baker Jr, P. Graves-Morris, G. Baker, and S. S. Baker. *Padé Approximants: Encyclopedia of Mathematics and Its Applications, Vol. 59 George A. Baker, Jr., Peter Graves-Morris*, volume 59. Cambridge University Press, 1996.
- [6] A. Berretti, A. Celletti, L. Chierchia, and C. Falcolini. Natural boundaries for area-preserving twist maps. *J. Statist. Phys.*, 66(5-6):1613–1630, 1992.
- [7] T. Blass and R. de la Llave. The analyticity breakdown for Frenkel-Kontorova models in quasi-periodic media: numerical explorations. *J. Stat. Phys.*, 150(6):1183–1200, 2013.
- [8] E. Bollt and J. Meiss. Breakup of invariant tori for the four-dimensional semi-standard map. *Phys. D*, 66:282–297, 1993.
- [9] R. P. Brent and H. T. Kung. Fast algorithms for manipulating formal power series. *J. Assoc. Comput. Mach.*, 25(4):581–595, 1978.
- [10] H. W. Broer, G. B. Huitema, and M. B. Sevryuk. *Quasi-Periodic Motions in Families of Dynamical Systems. Order Amidst Chaos*. Springer-Verlag, Berlin, 1996.
- [11] A. P. Bustamante and R. C. Calleja. Computation of domains of analyticity for the dissipative standard map in the limit of small dissipation. *Phys. D*, 395:15–23, 2019.
- [12] A. P. Bustamante and R. C. Calleja. Corrigendum and addendum to “Computation of domains of analyticity for the dissipative standard map in the limit of small dissipation” [Physica D 395 (2019) 15-23]. *Phys. D*, 417:Paper No. 132837, 7, 2021.
- [13] R. Calleja and A. Celletti. Breakdown of invariant attractors for the dissipative standard map. *CHAOS*, 20(1):013121, 2010.
- [14] R. Calleja, A. Celletti, and R. de la Llave. A KAM theory for conformally symplectic systems: efficient algorithms and their validation. *J. Differential Equations*, 255(5):978–1049, 2013.
- [15] R. Calleja, A. Celletti, and de la Llave R. KAM quasi-periodic solutions for the dissipative standard map. *Comm. Nonl. Sc. Num. Sim.*, 106:106111, 2022.
- [16] R. Calleja, A. Celletti, J. Gimeno, and R. de la Llave. Efficient and accurate KAM tori construction for the dissipative spin-orbit problem using a map reduction. *J. Nonlinear Sci.*, 32(1):Paper No. 4, 40, 2022.

- [17] R. Calleja, A. Celletti, J. Gimeno, and R. de la Llave. KAM quasi-periodic tori for the dissipative spin-orbit problem. *Commun. Nonlinear Sci. Numer. Simul.*, 106:Paper No. 106099, 22, 2022.
- [18] R. Calleja and R. de la Llave. A numerically accessible criterion for the breakdown of quasi-periodic solutions and its rigorous justification. *Nonlinearity*, 23(9):2029–2058, 2010.
- [19] R. C. Calleja. *Existence and persistence of invariant objects in dynamical systems and mathematical physics*. Ph.D. thesis, The University of Texas at Austin, 2009.
- [20] R. C. Calleja, A. Celletti, C. Falcolini, and R. de la Llave. An Extension of Greene’s Criterion for Conformally Symplectic Systems and a Partial Justification. *SIAM J. Math. Anal.*, 46(4):2350–2384, 2014.
- [21] R. C. Calleja, A. Celletti, J. Gimeno, and R. de la Llave. Accurate computations up to break-down of quasi-periodic attractors in the dissipative spin-orbit problem. *Preprint*, 2022.
- [22] M. Canadell and A. Haro. Computation of quasi-periodic normally hyperbolic invariant tori: algorithms, numerical explorations and mechanisms of breakdown. *J. Nonlinear Sci.*, 27(6):1829–1868, 2017.
- [23] A. Celletti and L. Chierchia. A constructive theory of Lagrangian tori and computer-assisted applications. In *Dynamics Reported*, pages 60–129. Springer, Berlin, 1995.
- [24] A. Celletti, C. Falcolini, and U. Locatelli. On the break-down threshold of invariant tori in four dimensional maps. *Regular and Chaotic Dynamics*, 9(3):227–253, 2004.
- [25] B. Chirikov. A universal instability of many-dimensional oscillator systems. *Phys. Rep.*, 52(5):264–379, 1979.
- [26] R. de la Llave, A. González, À. Jorba, and J. Villanueva. KAM theory without action-angle variables. *Nonlinearity*, 18(2):855–895, 2005.
- [27] R. de La Llave and S. Tompaidis. Nature of singularities for analyticity domains of invariant curves. *Physical Review Letters*, 73(11):1459, 1994.
- [28] R. De La Llave and S. Tompaidis. On the singularity structure of invariant curves of symplectic mappings. *Chaos: An Interdisciplinary Journal of Nonlinear Science*, 5(1):227–237, 1995.
- [29] C. Falcolini and R. de la Llave. A rigorous partial justification of Greene’s criterion. *J. Statist. Phys.*, 67(3-4):609–643, 1992.
- [30] A. M. Fox and J. D. Meiss. Greene’s residue criterion for the breakup of invariant tori of volume-preserving maps. *Phys. D*, 243:45–63, 2013.
- [31] A. M. Fox and J. D. Meiss. Computing the conjugacy of invariant tori for volume-preserving maps. *SIAM J. Appl. Dyn. Syst.*, 15(1):557–579, 2016.
- [32] J. Greene. A method for determining a stochastic transition. *Journal of Mathematical Physics*, 20(6):1183–1201, 1979.
- [33] J. M. Greene and I. C. Percival. Hamiltonian maps in the complex plane. *Phys. D*, 3(3):530–548, 1981.
- [34] A. Haro, M. Canadell, J.-L. Figueras, A. Luque, and J.-M. Mondelo. *The parameterization method for invariant manifolds*, volume 195 of *Applied Mathematical Sciences*. Springer, [Cham], 2016. From rigorous results to effective computations.
- [35] Y. A. Khinchin. *Continued fractions*. Dover Publications, 1997.
- [36] S.-H. Kim and S. Östlund. Simultaneous rational approximations in the study of dynamical systems. *Phys. Rev. A (3)*, 34(4):3426–3434, 1986.
- [37] A. N. Kolmogorov. On conservation of conditionally periodic motions for a small change in Hamilton’s function. *Dokl. Akad. Nauk SSSR (N.S.)*, 98:527–530, 1954. English translation in *Stochastic Behavior in Classical and Quantum Hamiltonian Systems (Volta Memorial Conf., Como, 1977)*, Lecture Notes in Phys., 93, pages 51–56. Springer, Berlin, 1979.
- [38] H. Kook and J. Meiss. Periodic orbits for reversible, symplectic mappings. *Phys. D*, 35:65–86, 1989.
- [39] R. S. MacKay. Greene’s residue criterion. *Nonlinearity*, 5(1):161–187, 1992.
- [40] J. D. Meiss and E. Sander. Birkhoff averages and the breakdown of invariant tori in volume-preserving maps. *Phys. D*, 428:Paper No. 133048, 20, 2021.

- [41] J. Moser. On invariant curves of area-preserving mappings of an annulus. *Nachr. Akad. Wiss. Göttingen Math.-Phys. Kl. II*, 1962:1–20, 1962.
- [42] J. Moser. Convergent series expansions for quasi-periodic motions. *Math. Ann.*, 169:136–176, 1967.
- [43] F. Schweiger. On the invariant measure for Jacobi-Perron algorithm. *Math. Pannon.*, 1(2):91–106, 1990.
- [44] S. Tompaidis. Approximation of invariant surfaces by periodic orbits in high-dimensional maps: some rigorous results. *Experiment. Math.*, 5(3):197–209, 1996.
- [45] S. Tompaidis. Numerical study of invariant sets of a quasiperiodic perturbation of a symplectic map. *Experiment. Math.*, 5(3):211–230, 1996.
- [46] W. Wenzel and J. C. Biham, O. Periodic orbits in the dissipative standard map. *Phys. Rev. A*, 43:6550–6557, 1991.

DEPARTMENT OF MATHEMATICS, UNIVERSITY OF ROMA TOR VERGATA, VIA DELLA RICERCA SCIENTIFICA 1, 00133 ROMA (ITALY)

Email address: bustamante@mat.uniroma2.it

DEPARTMENT OF MATHEMATICS, UNIVERSITY OF ROMA TOR VERGATA, VIA DELLA RICERCA SCIENTIFICA 1, 00133 ROMA (ITALY)

Email address: celletti@mat.uniroma2.it

DEPARTMENT OF MATHEMATICS, UNIVERSITY OF ROMA TOR VERGATA, VIA DELLA RICERCA SCIENTIFICA 1, 00133 ROMA (ITALY)

Email address: lhotka@mat.uniroma2.it